



저작자표시-비영리-변경금지 2.0 대한민국

이용자는 아래의 조건을 따르는 경우에 한하여 자유롭게

- 이 저작물을 복제, 배포, 전송, 전시, 공연 및 방송할 수 있습니다.

다음과 같은 조건을 따라야 합니다:



저작자표시. 귀하는 원저작자를 표시하여야 합니다.



비영리. 귀하는 이 저작물을 영리 목적으로 이용할 수 없습니다.



변경금지. 귀하는 이 저작물을 개작, 변형 또는 가공할 수 없습니다.

- 귀하는, 이 저작물의 재이용이나 배포의 경우, 이 저작물에 적용된 이용허락조건을 명확하게 나타내어야 합니다.
- 저작권자로부터 별도의 허가를 받으면 이러한 조건들은 적용되지 않습니다.

저작권법에 따른 이용자의 권리는 위의 내용에 의하여 영향을 받지 않습니다.

이것은 [이용허락규약\(Legal Code\)](#)을 이해하기 쉽게 요약한 것입니다.

[Disclaimer](#)

Thesis for the Degree of Master of Engineering

Synthesis of Quinoxaline-based Organic
Semiconducting Materials for
Optoelectronic Devices



by

Seok Woo Lee

Department of Industrial Chemistry

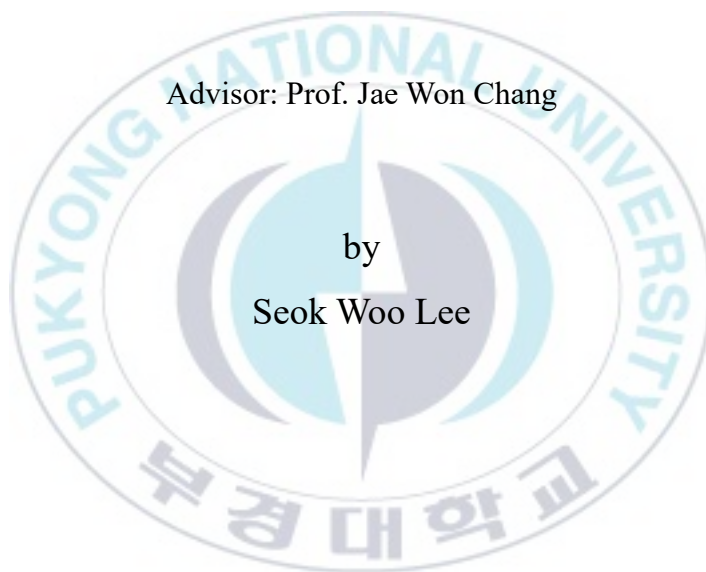
The Graduate School

Pukyong National University

February 2022

Synthesis of Quinoxaline-based Organic
Semiconducting Materials for
Optoelectronic Devices
(광전자소자용 퀴녹살린 기반
유기반도체 소재의 합성)

Advisor: Prof. Jae Won Chang



by

Seok Woo Lee

A thesis submitted in partial fulfillment of the requirements
for the degree of
Master of Engineering
in Department of Industrial Chemistry, The Graduate School,
Pukyong National University

February 2022

**Synthesis of Quinoxaline-based Organic Semiconducting
Materials for Optoelectronic Devices**

A dissertation

by

Seok Woo Lee

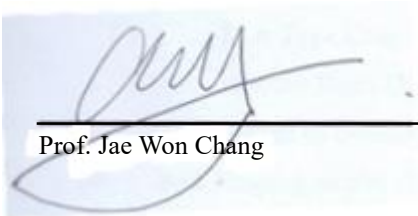
Approved by:



Prof. Bo Ram Lee



Prof. Young Eup Jin



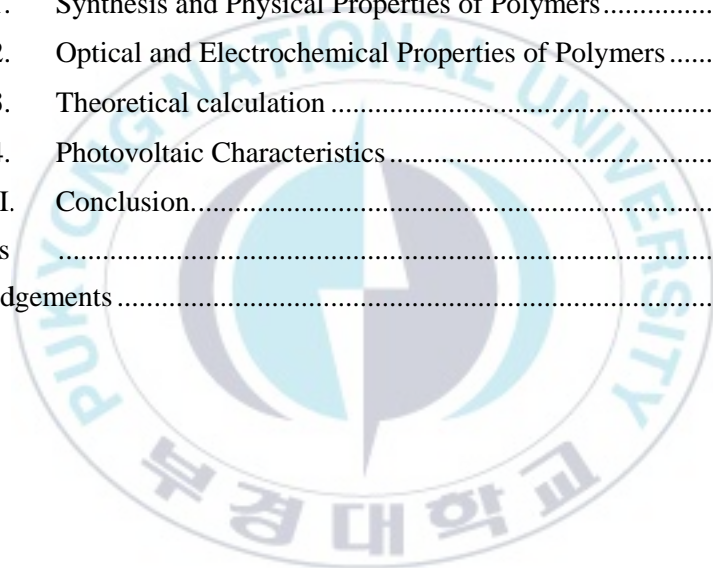
Prof. Jae Won Chang

February 25, 2022

Contents

Contents	i
List of Figures	iii
List of Tables	v
List of Schemes	vi
Abstract	vii
요약	viii
Chapter I. Introduction	1
I-1. Organic Semiconducting Materials	1
I-2. Classification of Organic Semiconductors.....	2
I-2.1. Organic field effect transistors (OFETs)	3
I-2.2. Organic Light-emitting Diodes (OLEDs).....	3
I-2.3. Organic Photovoltaics (OPVs)	3
I-3. Polymer Solar Cells (PSCs).....	4
I-4. Working Principles of Polymer Solar Cells.....	5
I-4.1. Absorption of photon and Exciton Formation.....	6
I-4.2. Exciton Dissociation.....	7
I-4.3. Charge Separation	7
I-4.4. Charge Extraction.....	8
I-5. Molecular Engineering Design of D-A Type Conjugated Polymers for Polymer Solar Cells.....	8
I-5.1. D-A Type Conjugated Polymers	9
I-5.2. Narrow Band-Gap Polymers	10
I-5.3. Target of Quinoxaline-based Structural Modifications	11
I-6. Bulk Heterojunction Polymer Solar Cells.....	12
I-7. Performance characteristics of Polymer Solar Cells.....	13
I-8. The Aim of Thesis	14

Chapter II. Position effect of Electron-Withdrawing Chlorine substituents on D-A Type Conjugated Polymers for Polymer Solar Cells	15
II-1. Experimental Section.....	15
II-1.1. Materials and Instruments	15
II-1.2. Synthesis of Monomers	16
II-1.3. General Procedure of Polymerization using Stille-Coupling Method with Palladium Catalyst	27
II-1.4. Fabrication and Analysis of Photovoltaic Devices.....	31
II-2. Result and Discussion.....	32
II-2.1. Synthesis and Physical Properties of Polymers.....	32
II-2.2. Optical and Electrochemical Properties of Polymers	33
II-2.3. Theoretical calculation	38
II-2.4. Photovoltaic Characteristics	41
Chapter III. Conclusion.....	48
References	49
Acknowledgements	52



List of Figures

Figure I-1. Representative organic semiconducting materials structures.....	2
Figure I-2. The normal (left) and inverted (right) device configurations with the light source passing through the device from the bottom side. ITO: indium tin oxide; HTL: hole transport layer; Al: active layer; ETL: electron transport layer	5
Figure I-3. The mechanism of the working principles of polymer solar cells.....	6
Figure I-4. Advantage of D-A type conjugated polymers	9
Figure I-5. Hybridization of molecular orbital energy levels of D-A type polymer via D-A intermolecular interactions	10
Figure I-6. The molecule designing of quinoxaline	11
Figure I-7. The device structure of bilayer-formed active layer (left) and BHJ formed active layer (right) devices.....	12
Figure I-8. J-V curves in the dark and illuminated PSC devices.....	13
Figure II-1. Chemical structure of PB-Q-Cl Series.....	29
Figure II-2. Device structure of PSCs.....	31
Figure II-3. UV-Visible spectra of polymer in (a) chloroform solution and (b) film-state on glass substrate (spectra are offset for clarity).....	35
Figure II-4. Cyclic voltammograms of PB-Q-Cl polymers.....	37
Figure II-5. Energy level diagram of all materials in the Conventional-type devices: HOMO was obtained from CV results and LUMO was obtained from optical band gap.....	38

Figure II-6. Frontier molecular orbitals of two-repeating unit models with energy levels calculated at the B3YLP/6-31G** level for PB-QCl Polymers.....40

Figure II-7. (a) J-V curve of PSCs under 1.0 sun condition and (b) EQE spectra of PSCs based on PB-Q-Cl Series43

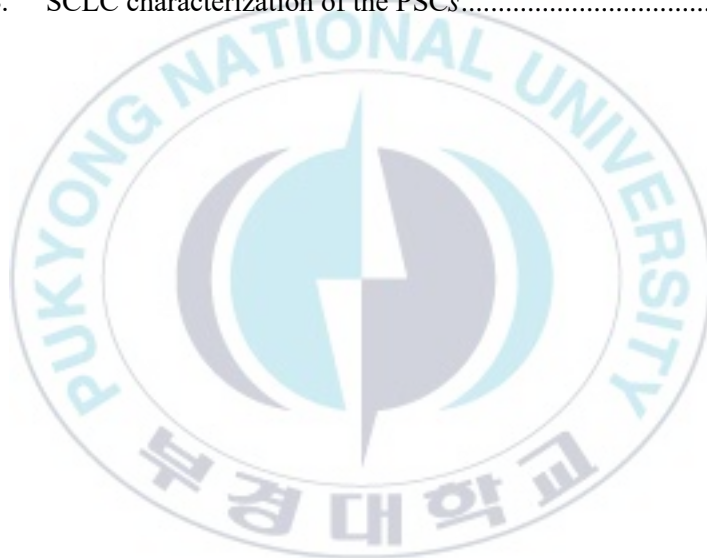
Figure II-8. J-V curves of (a) the electron-only and (b) hole-only devices.....45

Figure II-9. AFM images of **PB-Q-Cl** Seires polymer blend film with Y6.....46



List of Tables

Table II-1.	Molecular weight of the polymers.....	33
Table II-2.	Optical and electrochemical properties of the PB-Q-Cl Series.....	37
Table II-3.	Best photovoltaic parameters of the PSCs. Values in parentheses represent average value of photovoltaic parameters for each device	42
Table II-4.	SCLC characterization of the PSCs.....	44



List of Schemes

Scheme 1. Synthesis of PB-Q-CI Series.....30



Synthesis of Quinoxaline-based Organic Semiconducting Materials for Optoelectronic
Devices

Seok Woo Lee

Department of Industrial Chemistry, The Graduate School,
Pukyong National University

Abstract

In this study, the electron-withdrawing chlorine (Cl) substituents are selectively incorporated into the quinoxaline unit of D–A-type conjugated polymers to investigate their position effects on the photovoltaic properties of the polymers. To construct the D-A type polymeric architecture, electron-donating benzodithiophene (BDT) and long alkyl chain-substituted phenyl units and electron-withdrawing chlorine units are directly linked to the horizontal and vertical directions of the quinoxaline acceptor, respectively. After confirming the chemical structural, optical, and electrochemical properties of the resultant Cl-substituted polymers, labeled as **PB-Q**, **PB-Q-4Cl** and **PB-Q-5Cl**, respectively. Photovoltaic performances are discovered that the maximum power conversion efficiency of **PB-Q-4Cl** is 12.95%, whereas that of **PB-Q-5Cl** is limited to 11.82%. Therefore, the photovoltaic performance of quinoxaline-based D–A-type polymers is significantly affected by the position of electron-withdrawing substituents.

광전지소자용 유기반도체 소재의 합성

Seok Woo Lee

부경대학교 대학원 공업화학과

요약

본 연구에서는 서로 다른 위치에 전자 받게 기능성 그룹이 도입된 공액형 고분자들을 합성한 뒤, 이들을 대표적인 유기 반도체 소자인 태양전지 소자에 적용하여 광전지 특성을 연구하였다. Benzodithiophene (BDT) 전자 주게와 서로 다른 위치의 염소 그룹이 도입된 퀴녹살린의 전자 받게 반복단위에 기반하여 고분자 구조를 설계 및 합성하였다. 해당 고분자의 경우, 모든 고분자의 전자 주게 반복단위에 염소 그룹이 도입되었으며 전자 받게 반복단위에 염소 그룹이 도입되지 않은 PB-Q, 해당 전자 받게의 퀴녹살린의 반복단위에서 티오펜 결까지 그룹의 4번위치에 염소 그룹을 추가 도입한 PB-Q-4Cl 그리고 5번 위치에 염소 그룹을 추가 도입한 PB-Q-5Cl을 각각 합성하였다. 해당 고분자의 광전지 특성은 ITO/PEDOT:PSS/Active layer/PDINO/Al의 배치를 가지는 conventional-type 구조의 소자에서 4번 위치에 염소 그룹을 도입한 퀴녹살린 반복단위 고분자인 PB-Q-4Cl가 염소 그룹의 효율적인 위치적 도입을 통해 최고 효율 12.95%로 측정되었다. 하지만, 5번 위치에 염소 그룹을 도입한 퀴녹살린 반복단위 고분자인 PB-Q-5Cl에서는 5번위치의 염소 그룹 도입이 광활성층에 악영향을 미치며 염소 그룹을 도입하지 않은 고분자보다 하락된 태양전지 효율 경향성을 보였다. 따라서, 이러한 결과는 향후 다른 위치에 도입된 전자 받게 기능성 그룹이 도입된 퀴녹살린 기반 공액형 고분자의 구조-물성 간 상관관계 연구에 활용될 수 있을 것이다.

Chapter I. Introduction

I-1. Organic Semiconducting Materials

In recent several decades, the development of organic semiconducting materials has been leading to paving the way toward the growth of high-performance organic semiconductors [1–3]. Comparing to the inorganic semiconductor, the organic conductors provide the advantages such as the lightweight, flexibility and low-cost. Hence, it is important to design and synthesize new organic semiconducting materials for acquiring the high-performance organic semiconductors. Among of numerous candidates, the π -conjugated molecule is the most prominent and plays a very important role. Recently, improving the properties of the energy of frontier molecular orbitals and the distribution of the orbitals through structural modification of molecules is an essential element of organic semiconducting materials. For example, in each case, the energy level of the highest occupied molecular orbital (HOMO) depends on the electron density and delocalization of the π electrons through the molecular backbones. It has a great effect on optical/electrochemical factors such as light absorption/emission and charge extraction/injection of molecules, and can be a key point to improve the performance of organic semiconductor devices. Until now, organic semiconducting materials are developing through various structural modification and further development is expected.

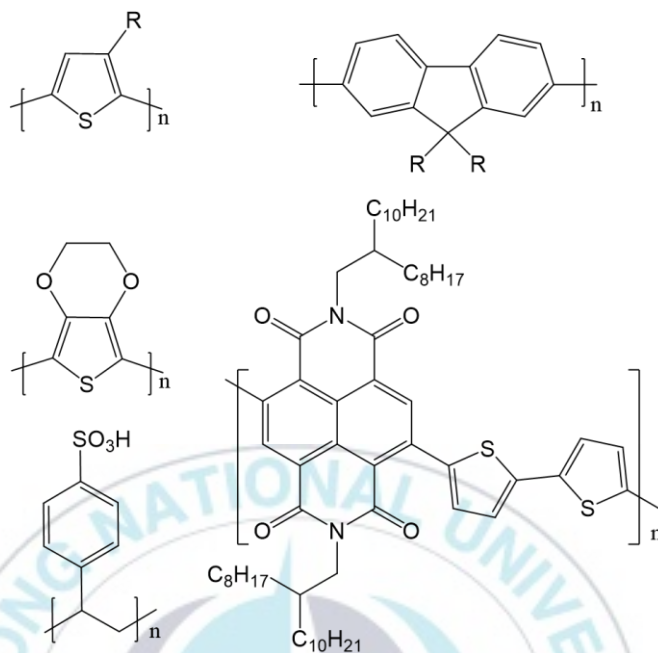


Figure I-1. Representative organic semiconducting materials structures

I-2. Classification of Organic Semiconductors

Organic semiconducting materials are being applied to organic semiconductors of various devices by utilizing their unique properties. In general, organic semiconductors operate by controlling the *n*-type and *p*-type characteristics of molecules [4,5]. The following properties are expressed by the intramolecular structure and are introduced into the structure of small molecules or the repeating unit of a polymers to improve various organic semiconductor properties. Representative devices include the organic field effect transistors (OFETs), organic light-emitting diodes (OLEDs), and organic photovoltaic devices.

I-2.1. Organic field effect transistors (OFETs)

First, an organic field-effect transistor (OFET) is one of the representative organic semiconductor devices that use organic semiconducting materials for channels. Generally, it utilizes charge transport in organic semiconducting materials. The charge transport in organic semiconducting materials depends on a combination of molecule's intrachain polaron conjugation and intermolecular charge carrier hopping between adjacent molecule chains [6]. The performance of the OFETs is mainly determined by the charge mobility, and studies are being conducted to improve the performance of organic semiconducting materials as well.

I-2.2. Organic Light-emitting Diodes (OLEDs)

Second, even in the case of an organic light-emitting diodes (OLEDs), it is one of the representative organic semiconductor devices using an organic semiconducting materials as light emission or charge transport layer. Generally, it utilizes the electroluminescence and carrier transport properties in organic semiconducting materials [7]. The performance of the OLEDs is mainly determined by the turn-on voltage, luminance, luminous efficiency, and external quantum efficiency.

I-2.3. Organic Photovoltaics (OPVs)

Third, even in the case of an organic photovoltaics (OPVs), it is one of the

representative organic semiconductor devices using an organic semiconducting materials as light absorption. OPVs work by photon absorption and exciton formation in the active layer. Hence, the performance of OPVs is mainly determined by the power conversion efficiency (PCE) [8–10].

I-3. Polymer Solar Cells (PSCs)

Since the photovoltaic effect was discovered, various organic molecules have been utilized in the photoactive layer. Among them, polymer solar cells are being actively studied due to their excellent properties. In particular, the *p*-type polymeric donor has been actively studied for a long time, and the performance of the device has been rapidly improved through numerous research results [11–13]. Recently, even in the case of an *n*-type polymeric acceptor, research is being conducted showing high-performance device.

The *p*-type polymeric donor, which has been studied for a long time, is the most important organic semiconducting materials among the photoactive layer components of PSCs. Similarly, in this study, electron-withdrawing groups of different positions were incorporated into the organic semiconducting materials and applied to polymer solar cells, and the related simple theories will be explained in the following order of contents.

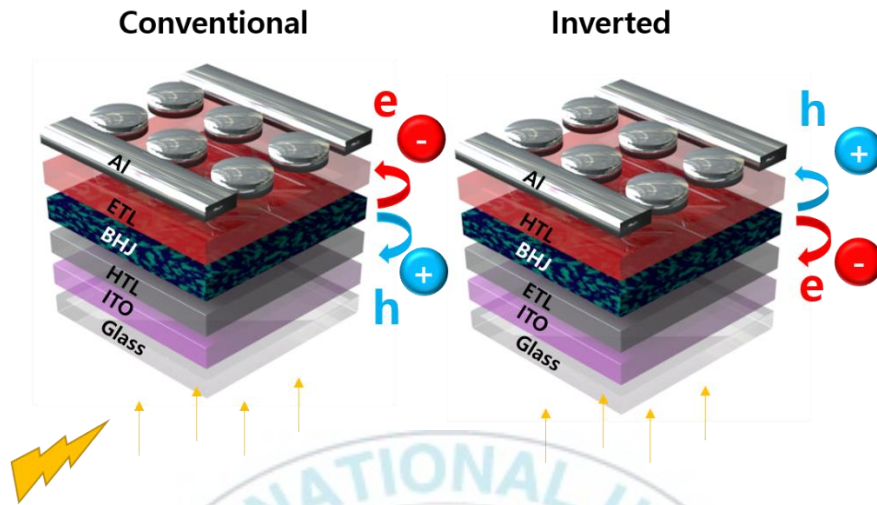


Figure I-2. The normal (left) and inverted (right) device configurations with the light source passing through the device from the bottom side. ITO: indium tin oxide; HTL: hole transport layer; AI: active layer; ETL: electron transport layer.

I-4. Working Principles of Polymer Solar Cells

PSCs driven by sunlight produce renewable energy through four major steps [14,15]. The energy of sunlight is absorbed by the *p*-type donor polymer in the photoactive layer, and excitons, which are electron and hole pairs, are formed. Therefore, in order to fabricate a high-performance polymer solar cell, it is important to develop the characteristics of organic semiconducting materials based on following process. In particular, a strategy to match the energy level between the *p*-type polymeric donor and the *n*-type acceptor is promising. This is closely related to the operating principle of the polymer solar cell to be described in the contents.

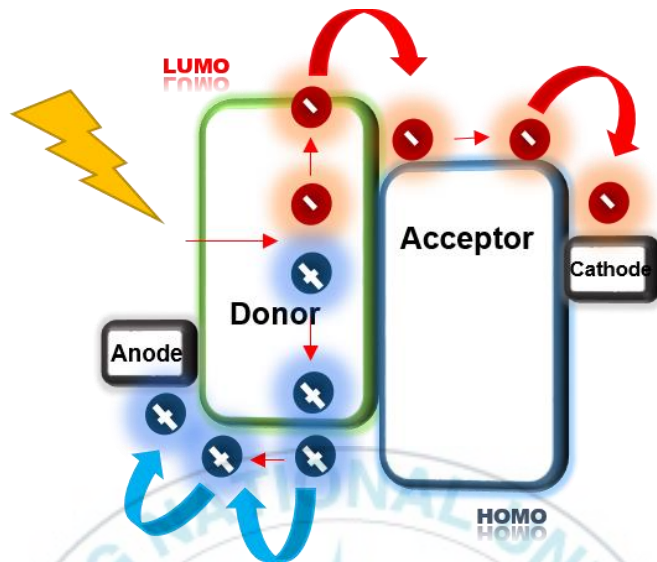


Figure I-3. The mechanism of the working principles of polymer solar cells

I-4.1. Absorption of photon and Exciton Formation

When a *p*-type polymeric donor absorbs sunlight, excitons are produced by photons in the sunlight. Due to the low dielectric constant of organic semiconducting materials, electrons and holes can be generated from photons by coulombic force. Unlike inorganic semiconducting materials that have a large dielectric constant, organic semiconducting materials generally have a low dielectric constant. So, the exciton containing the strong bond of electron and hole pair is produced. This produced exciton needs another step to separate it into the free electron and hole. In addition, to convert efficiently sunlight into energy, this is a step to prove that the *p*-type polymeric donor must have high absorption coefficient to reduce photon

reflectance and produce a lot of energy.

I-4.2. Exciton Dissociation

After the exciton is produced, an electron is excited from the p-type polymeric donor's HOMO to the lowest unoccupied molecular orbital (LUMO). In general, the generated exciton has a binding energy of 0.3-1 eV and must be overcome and dissociated. The dissociation of excitons occurs at the interface between the p-type polymeric donor and the n-type acceptor, which proceeds as a diffusion process. The efficiency of exciton diffusion can be calculated through the following equation :

$$L_D = (D\tau)^{1/2}$$

Where D is the diffusion coefficient and τ is the exciton lifetime.

I-4.3. Charge Separation

Once the exciton arrives the donor/acceptor interface it should undergo separation into free charges. The charge separation step takes place at the interface of donor and acceptor with different electron affinities and ionization potentials. Firstly, the electron transfers from the exciton to the LUMO of the n-type acceptor. At this time, it is in the form of D^+/A^- called charge transfer state (CT). Charges are completely separated by coulombic attraction due to the properties of p-type and n-type properties of organic semiconducting materials. So, electrons and holes are produced.

I-4.4. Charge Extraction

After free electrons and holes are created, they move to each electrode according to the work function, respectively. The free electrons separated from the exciton move from the donor's LUMO to the acceptor's LUMO to the cathode through high electron affinity. In the case of holes, they remain in the donor with a low ionization potential and are collected into the anode. In order to proceed with this step efficiently, it is applied to improve the device performance by controlling the properties of the organic semiconducting material to suppress the recombination of the generated charge.

I-5. Molecular Engineering Design of D-A Type Conjugated Polymers for Polymer Solar Cells

With the aim to obtain the high-performance polymer solar cells, designing and synthesizing the suitable conjugated polymer is an essential factor. The *p*-type conjugated polymer is expected to have a high extinction coefficient, an appropriate energy level with an acceptor and a well-formed morphology. In addition, the broad absorption region from conjugated polymer can be achieved by controlling the optical bandgap of the energy level. While an appropriate energy level with an acceptor is highly correlated with the energy loss. Also, morphology is related with the charge carrier mobility. Like this, several strategies have been studied to achieve

the high-performance PSCs.

I-5.1. D-A Type Conjugated Polymers

For fabricating high-performance PSCs, *p*-type polymeric donors have been intensively investigated with alternating electron-donating and accepting units along their main backbones. As shown in **Figure I-3**, it is widely known that the introduction of an alternating D-A structure into a *p*-type polymer donor improves optical and electrochemical properties, and that the acceptor and photoactive layer can be formed more efficiently by utilizing the difference in electron affinity. Therefore, using the following *p*-type polymeric donor, a polymer solar cell performance of about 18% has been recently reached [16–19].

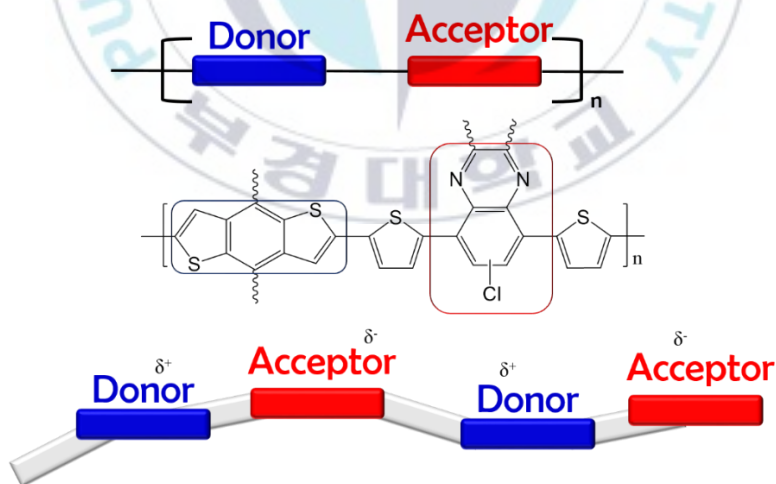


Figure I-4. Advantage of D-A type conjugated polymers

I-5.2. Narrow Band-Gap Polymers

The conjugated polymer's HOMO/LUMO energy levels strongly depend on the degree of electron delocalization with effective conjugation length (ECL). So, the hybridization of molecular orbitals in energy levels are not easily predictable. Therefore, in order to realize a high-performance PSCs, a polymer repeating unit with a narrow bandgap has been continuously studied.

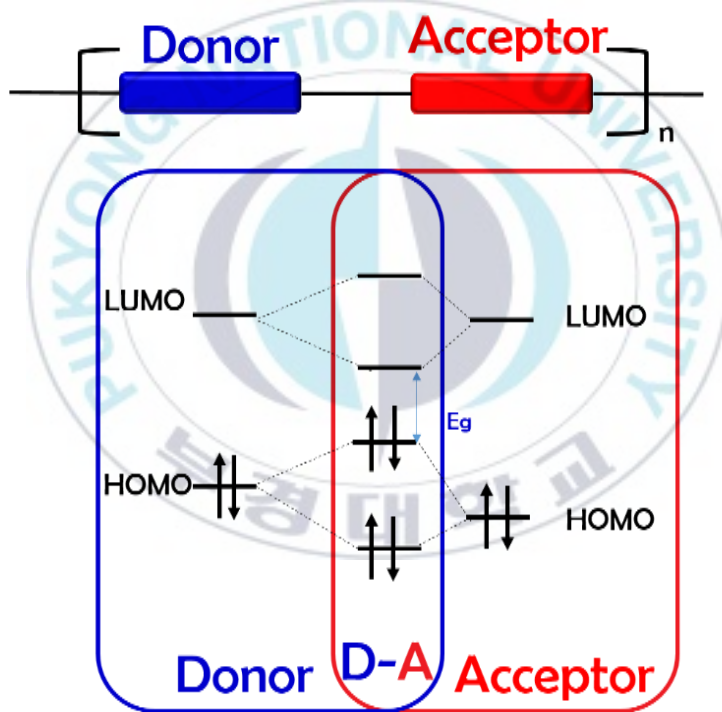


Figure I-5. Hybridization of molecular orbital energy levels of D-A type polymer *via* D-A intermolecular interactions

I-5.3. Target of Quinoxaline-based Structural Modifications

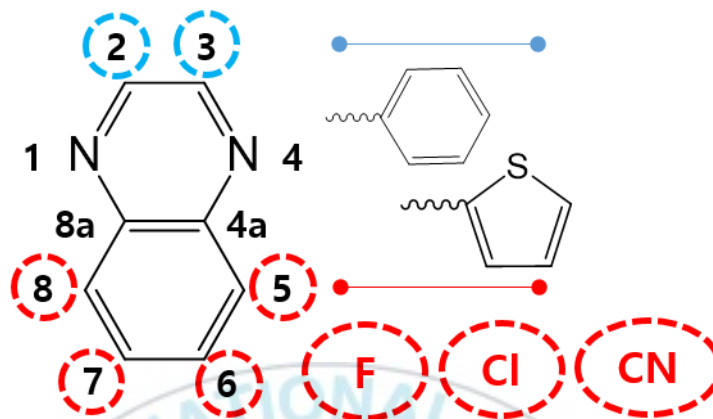


Figure I-6. The molecule designing strategy of quinoxaline

In order to improve the advantages of the aforementioned D-A type conjugated polymers, recently, there are often studies that introduce a quinoxaline acceptor unit to form a repeating unit. The biggest advantage of quinoxaline (Qx) is that it can achieve suitable properties through molecular structure modification. Quinoxaline is an accepting main backbone with many positions available. Thus, intensive studies have been conducted to control the properties of quinoxaline by introducing aromatic ring side chains or functional groups in the horizontal and vertical direction. The following strategy can design infinite chemical structures in the repeating unit composition of D-A type conjugated polymer and systematically improve the efficiency of PSCs.

I-6. Bulk Heterojunction Polymer Solar Cells

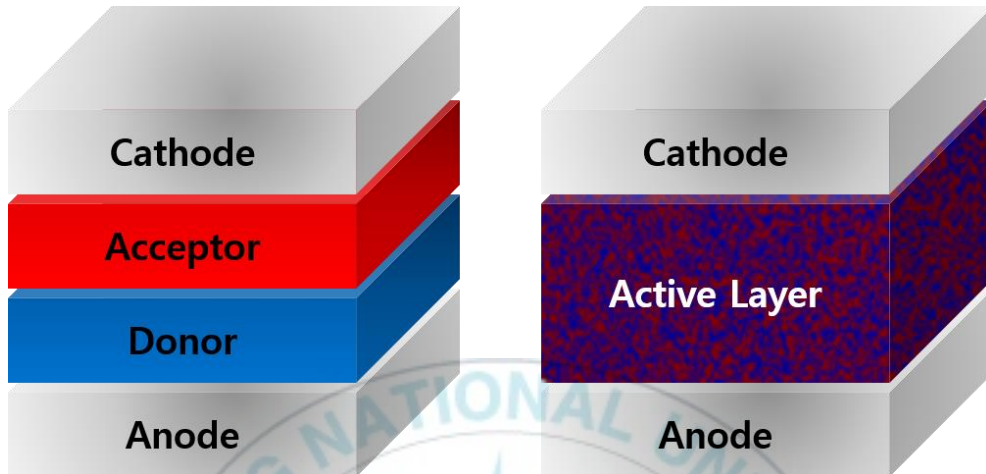


Figure I-7. The device structure of bilayer-formed active layer (left) and BHJ formed active layer (right) devices.

In the early days of research on PSCs, donor and acceptor layers were constructed in the form of a bilayer. However, to construct a high-performance PSCs, a layer was formed by blending a donor and an acceptor. Therefore, a bulk heterojunction (BHJ) type PSCs are emerged. The BHJ network can effectively reduce the interfacial distance between donor and acceptor. This suggests that energy loss can be minimized and the potential for energy generation can be maximized. Therefore, it is important to smooth the blending morphology of donor and acceptor, and it can have a great influence on the performance of PSCs [20].

I-7. Performance characteristics of Polymer Solar Cells

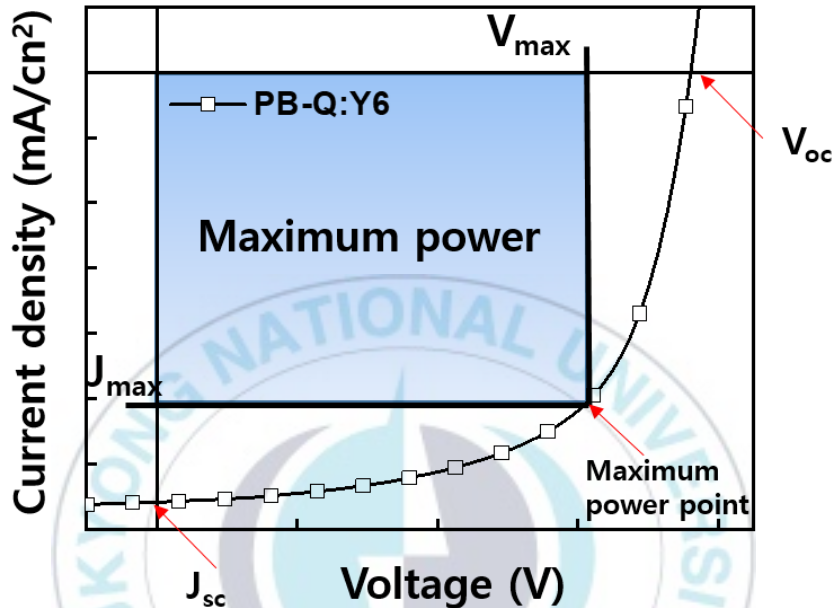


Figure I-8. J-V curves in the dark and illuminated PSC devices

Power conversion efficiency (PCE) is the most crucial metric used to evaluate polymer solar cells performance [21,22].

It is defined as below formula :

$$PCE = \frac{V_{oc} \times J_{sc} \times FF}{P_{in}}$$

As in the above equation, the efficiency parameters of the polymer solar cell include V_{oc} related to open-circuit voltage, J_{sc} related to short-circuit current and FF .

First, V_{oc} is defined as the maximum potential produced by the device with the condition that the device is open circuit which means the J_{sc} value is zero. there is no

current circulating the circuit. Second, J_{sc} is defined as the maximum photocurrent density produced by the device with the condition that means the V_{oc} value is zero. Finally, FF is defined as the ratio between the maximum power as the output of device to the J_{sc} and V_{oc} value.

It could be expressed in the mathematical equation below.

$$FF = \frac{V_m \times J_m}{V_{oc} \times J_{sc}}$$

I-8. The Aim of Thesis

The aim of this thesis is to obtain the insight of the chemical structure design and synthesis of the new D-A type conjugated polymers and the correlation between the chemical engineering design with its photovoltaic properties applied in the photovoltaic device. In this study, three different polymers were synthesized. The polymer was constructed from the BDT derivatives and chlorine-substituted 2,3-dithenylquinoxaline (DTQ) with the different position effect. This enhanced photovoltaic performance of the photovoltaic device with the polymer with a C-4 position chlorine atom can be attributed to the increase in the charge mobility, charge generation and dissociation, molecular ordering, and suppression of unfavorable recombination kinetics. Therefore, we investigate the incorporation of a chlorine atom on quinoxaline unit as horizontal direction in photovoltaic properties.

Chapter II. Position effect of Electron-Withdrawing Chlorine substituents on D-A Type Conjugated Polymers for Polymer Solar Cells

II-1. Experimental Section

II-1.1. Materials and Instruments

Iodine, 3-bromothiophene, Pd(PPh₃)₂Cl₂, oxalyl chloride, tri(*o*-tolyl)phosphine, and aluminium chloride were purchased from TCI chemicals. All other reagent and solvents were purchased from Sigma Aldrich Chemical Co., Inc. 5-(bromomethyl)undecane [23] and 5-chloro-4,7-di(thiophen-2-yl)benzo[*c*][1,2,5]thiadiazole (14) were produced according to previously similar reported method [24]. ¹H and ¹³C nuclear magnetic resonance (NMR) spectra were measured with a JEOL JNM ECP-400 spectrometer. UV-visible spectra were recorded on a Lamda 365 spectrophotometer. Matrix-assisted laser desorption/ionization time-of-flight (MALDI-TOF) spectroscopy was conducted by using a Bruker Ultraflex spectrometer. Gel Permeation Chromatography was analyzed in tetrahydrofuran (THF) by using an Agilent 1200S/mini DAWN TREOS. Cyclic voltammetry (CV) measurements were carried out by using a VersaSTAT3 potentiostat (Princeton Applied Research) with tetrabutylammonium hexafluorophosphate (0.1M, Bu₄NPF₆) as the electrolyte in acetonitrile. For CV measurements, a glassy carbon electrode coated with the polymer and a platinum

wire were used as the working and counter electrode, respectively. A silver wire was used as a pseudo-reference electrode with a ferrocene(Fc)/ferrocenium(Fc⁺) external standard.

II-1.2. Synthesis of Monomers

II-1.2.1. 2-(2-butylloctyl)thiophene (3)

In a two-neck round bottom flask under N₂ protection, thiophene (**1**, 2 equiv., 9.98 mmol) was dissolved in anhydrous tetrahydrofuran (THF) and cooled down to -78°C. After that, *n*-Butyllithium (2.5 M in Hexane, 2 equiv., 9.98 mmol) was added dropwisely and stirred for 1 h. And then, 5-(bromomethyl)undecane (1 equiv, 4.99 mmol) was added. The mixture was then stirred overnight at room temperature (RT) and extracted with dichloromethane. The organic layer was collected and dried over magnesium sulfate. The solvents were removed using rotary evaporator and the crude product was purified by column chromatography using hexane as eluent. Yield = 71% (colourless liquid). ¹H-NMR (400 MHz, CDCl₃) δ 7.09 (dd, J = 5.0, 1.4 Hz, 1H), 6.90 (dd, J = 5.0, 3.7 Hz, 1H), 6.73 (q, J = 1.4 Hz, 1H), 2.74 (d, J = 6.9 Hz, 2H), 1.60 (s, 1H), 1.26-1.24 (m, 16H), 0.88-0.84 (m, 6H). ¹³C-NMR (100 MHz, CDCl₃) δ 144.4, 126.6, 125.1, 123.0, 40.1, 34.3, 33.2, 32.9, 32.0, 29.7, 28.9, 26.6, 23.1, 22.8, 14.3, 14.2.

II-1.2.2. *2-(2-butyloctyl)-3-chlorothiophene (4)*

In a two-neck round bottom flask under N₂ protection, 3-chlorothiophene (**2**, 1 equiv., 25.3 mmol) was dissolved in anhydrous THF and cooled down to -78°C. After that, lithium diisopropylamide solution (2.0 M in THF/Heptane/ethylbenzene, 1.2 equiv., 30.36 mmol) was added drop-wisely and stirred for 1 h. And then, 5-(bromomethyl)undecane (1 equiv, 25.3 mmol) was added. The mixture was then stirred overnight at room temperature and extracted with dichloromethane. The organic layer was collected and dried over magnesium sulfate. The solvents were removed using rotary evaporator and the crude product was purified by column chromatography using hexane as eluent. Yield = 66% (colourless liquid). ¹H-NMR (400 MHz, CDCl₃) δ 7.08 (d, J = 5.0 Hz, 1H), 6.83 (d, J = 5.5 Hz, 1H), 2.70 (d, J = 6.9 Hz, 2H), 1.65 (s, 1H), 1.27-1.24 (m, 17H), 0.88-0.84 (m, 6H). ¹³C-NMR (100 MHz, CDCl₃) δ 137.0, 127.4, 122.7, 122.1, 39.5, 33.3, 33.0, 32.2, 32.0, 29.7, 28.8, 26.5, 23.1, 22.8, 14.2.

II-1.2.3. *3-(2-butyloctyl)thiophene (6)*

In an oven-dried two-neck round bottom flask with a condenser under N₂ protection, the flask was charged with magnesium-turnings (2.75 equiv., 87.72 mmol) and a tip of Iodine. The flask was heated with a heat-gun. And then, 5-(bromomethyl)undecane (1.5 equiv., 47.85 mmol) was dissolved in anhydrous diethyl ether and added dropwise into the flask. After that, the mixture was refluxed

for 3h. After previous reaction, one more oven-dried two-neck round bottom flask was prepared and charged with Dichloro[1,3-bis(diphenylphosphino)propane]nickel(II) (0.003 equiv., 0.0957 mmol) and 3-bromothiophene (**1**, 1 equiv., 31.9 mmol) was charged with anhydrous diethyl ether. The flask was put into an ice bath. The Grignard-reagent was carefully injected, and the flask left to stand overnight in room temperature. After all reaction, a diluted HCl solution was slowly added and stirred for 30 min. The mixture was extracted with diethyl ether. The organic layer was collected and dried over magnesium sulfate. The solvents were removed using rotary evaporator and the crude product was purified by column chromatography using hexane as eluent. Yield = 51% (colourless liquid). ¹H-NMR (400 MHz, CDCl₃) δ 7.21 (q, J = 2.6 Hz, 1H), 6.89-6.86 (m, 2H), 2.54 (d, J = 6.9 Hz, 2H), 1.58 (t, J = 5.7 Hz, 1H), 1.26-1.23 (m, 16H), 0.87 (t, J = 3.2 Hz, 6H). ¹³C-NMR (100 MHz, CDCl₃) δ 142.0, 128.9, 124.8, 120.7, 39.0, 34.8, 33.4, 33.1, 32.0, 29.8, 29.0, 26.7, 23.1, 22.8, 14.2.

II-1.2.4. 3-(2-butylloctyl)-2-chlorothiophene (7)

In a round bottom flask under N₂ protection, 3-(2-butylloctyl)thiophene (**4**, 1 equiv., 11 mmol) was dissolved in anhydrous THF at RT. After that, N-chlorosuccinimide (1.05 equiv., 11.55 mmol) was added and stirred overnight at RT. And then, the mixture was extracted with dichloromethane. The organic layer was collected and dried over magnesium sulfate. The solvents were removed using rotary evaporator

and the crude product was purified by column chromatography using hexane as eluent. Yield = 62% (colourless liquid). $^1\text{H-NMR}$ (400 MHz, CDCl_3) δ 6.99 (d, J = 5.5 Hz, 1H), 6.74 (d, J = 5.5 Hz, 1H), 2.48 (d, J = 6.9 Hz, 2H), 1.61 (s, 1H), 1.23 (s, 16H), 0.86 (t, J = 6.6 Hz, 7H). $^{13}\text{C-NMR}$ (100 MHz, CDCl_3) δ 138.5, 128.6, 125.0, 121.9, 38.6, 33.4, 33.1, 32.6, 32.0, 29.7, 28.8, 26.6, 23.1, 22.8, 14.2.

II-1.2.5. 1,2-bis(5-(2-butyloctyl)thiophen-2-yl)ethane-1,2-dione

(8)

A solution of oxalyl chloride (1 equiv., 1.7 mmol) in dichloromethane was added in succession to a solution of aluminium chloride (4 equiv., 6.8 mmol) in dichloromethane cooled down to 0 °C. And then, 2-(2-butyloctyl)thiophene (**5**, 2.1 equiv., 3.57 mmol) was added dropwise. The mixture was heated to RT and stirred overnight. And then, the mixture was extracted with dichloromethane. The organic layer was collected and dried over magnesium sulfate. The solvents were removed using rotary evaporator and the crude product was purified by column chromatography using MC/hexane (1/75, v/v) as eluent. Yield : 42% (yellow oil). $^1\text{H-NMR}$ (400 MHz, CDCl_3) δ 7.85 (d, J = 4.1 Hz, 2H), 6.84 (d, J = 4.1 Hz, 2H), 2.80 (d, J = 6.4 Hz, 4H), 1.67 (s, 2H), 1.26-1.23 (m, 32H), 0.87-0.84 (m, 12H). $^{13}\text{C-NMR}$ (100 MHz, CDCl_3) δ 182.7, 159.0, 137.8, 136.9, 127.5, 40.2, 35.3, 33.3, 32.9, 31.9, 29.7, 28.9, 26.6, 23.0, 22.8, 14.2.

II-1.2.6. 1,2-bis(5-(2-butyloctyl)-4-chlorothiophen-2-yl)ethane-1,2-dione (9)

The method to produce 1,2-bis(5-(2-butyloctyl)-4-chlorothiophen-2-yl)ethane-1,2-dione (**9**) was similar to the method used to produce compound **8**. Instead of 2-(2-butyloctyl)thiophene (**5**), 2-(2-butyloctyl)-3-chlorothiophene (**6**, 3.56 mmol) was used as the starting material. The crude product was purified by column chromatography using MC/hexane (1/80, v/v) as eluent. Yield : 43% (yellow oil). ¹H-NMR (400 MHz, CDCl₃) δ 7.86 (s, 2H), 2.78 (d, J = 7.3 Hz, 4H), 1.74 (s, 2H), 1.28-1.24 (m, 32H), 0.87-0.84 (m, 13H). ¹³C-NMR (100 MHz, CDCl₃) δ 180.4, 151.9, 137.3, 133.9, 125.5, 39.6, 33.4, 33.0, 31.9, 29.6, 28.8, 26.5, 23.0, 22.7, 14.2.

II-1.2.7. 1,2-bis(4-(2-butyloctyl)-5-chlorothiophen-2-yl)ethane-1,2-dione (10)

The method to produce 1,2-bis(4-(2-butyloctyl)-5-chlorothiophen-2-yl)ethane-1,2-dione (**10**) was similar to the method used to produce compound **8**. Instead of 2-(2-butyloctyl)thiophene (**5**), 3-(2-butyloctyl)-2-chlorothiophene (**7**, 4 mmol) was used as the starting material. The crude product was purified by column chromatography using MC/hexane (1/80, v/v) as eluent. Yield : 48% (yellow oil). ¹H-NMR (400 MHz, CDCl₃) δ 7.80 (s, 2H), 2.51 (d, J = 7.3 Hz, 4H), 1.63 (s, 2H), 1.25-1.22 (m, 32H), 0.87-0.83 (m, 13H). ¹³C-NMR (100 MHz, CDCl₃) δ 180.0, 141.0, 140.3, 138.6, 133.2,

38.5, 33.3, 33.0, 32.6, 31.9, 29.7, 28.8, 26.5, 23.1, 22.7, 14.2.

II-1.2.8. 5-chlorobenzo[c][1,2,5]thiadiazole (12)

5-chlorobenzo[c][1,2,5]thiadiazole (**12**) was produced according to previously reported method. ¹H-NMR (400 MHz, CDCl₃) δ 8.01 (t, J = 1.4 Hz, 1H), 7.93 (d, J = 8.7 Hz, 1H), 7.54 (dd, J = 9.4, 2.1 Hz, 1H).

II-1.2.9. 4,7-dibromo-5-chlorobenzo[c][1,2,5]thiadiazole (13)

4,7-dibromo-5-chlorobenzo[c][1,2,5]thiadiazole (**13**) was produced according to previously reported method. ¹H-NMR (400 MHz, CDCl₃) δ 7.93 (d, J = 0.9 Hz, 1H).

II-1.2.10. 5-chloro-4,7-di(thiophen-2-yl)benzo[c][1,2,5]thiadiazole (14)

5-chloro-4,7-di(thiophen-2-yl)benzo[c][1,2,5]thiadiazole (**14**) was produced according to previously reported method. ¹H-NMR (400 MHz, CDCl₃) δ 8.11 (d, J = 3.7 Hz, 1H), 7.95 (s, 1H), 7.75 (dd, J = 3.5, 1.0 Hz, 1H), 7.58 (dd, J = 5.0, 0.9 Hz, 1H), 7.50 (dd, J = 5.0, 0.9 Hz, 1H), 7.23-7.20 (m, 2H).

II-1.2.11. 2,3-bis(5-(2-butyloctyl)thiophen-2-yl)-6-chloro-5,8-

di(thiophen-2-yl)quinoxaline (15)

In a round bottom flask, 5-chloro-4,7-di(thiophen-2-yl)benzo[c][1,2,5]thiadiazole (**14**, 1 equiv., 0.83 mmol) and Zinc powder (20 eq., 12.42 mmol) were mixed together with acetic acid (20 mL) at 80°C and stirred for 4h. After that, the Zinc powder was filtered off. 1,2-bis(5-(2-butyloctyl)thiophen-2-yl)ethane-1,2-dione (**8**, 1 equiv., 0.83 mmol) was then added into the filtrate and the mixture was stirred overnight at 110°C. It was cooled down to room temperature. And then, the mixture was extracted with dichloromethane. The organic layer was collected and dried over magnesium sulfate. The solvents were removed using rotary evaporator and the crude product was purified by column chromatography using MC/hexane (1/60, v/v) as eluent. Yield : 42% (yellow-orange oil). ¹H-NMR (400 MHz, CDCl₃) δ 8.08 (s, 1H), 7.87 (dd, J = 3.9, 1.1 Hz, 1H), 7.60 (dd, J = 5.0, 1.4 Hz, 1H), 7.55-7.52 (m, 2H), 7.40 (d, J = 3.7 Hz, 1H), 7.35 (d, J = 3.7 Hz, 1H), 7.20 (ddd, J = 11.9, 5.0, 3.7 Hz, 2H), 6.68 (d, J = 3.7 Hz, 1H), 6.61 (d, J = 3.9 Hz, 1H), 2.78 (dd, J = 29.5, 6.6 Hz, 4H), 1.67 (d, J = 26.1 Hz, 2H), 1.32-1.26 (m, 32H), 0.91-0.85 (m, 12H). ¹³C-NMR (100 MHz, CDCl₃) δ 150.2, 149.8, 145.8, 144.6, 139.5, 139.4, 139.0, 137.4, 135.0, 134.5, 134.1, 132.2, 130.9, 130.1, 130.0, 129.5, 129.2, 128.4, 128.0, 127.5, 126.9, 126.1, 125.9, 125.8, 40.0, 39.9, 34.8, 34.8, 33.4, 33.4, 33.0, 33.0, 32.0, 29.8, 29.0, 26.7, 23.1, 23.1, 22.8, 14.3, 14.3.

II-1.2.12. 2,3-bis(5-(2-butyloctyl)-4-chlorothiophen-2-yl)-6-chloro-5,8-di(thiophen-2-yl)quinoxaline (16)

The method to produce 2,3-bis(5-(2-butyloctyl)-4-chlorothiophen-2-yl)-6-chloro-5,8-di(thiophen-2-yl)quinoxaline (**16**) was similar to the method used to produce **15**. Instead of 1,2-bis(5-(2-butyloctyl)thiophen-2-yl)ethane-1,2-dione (**8**), 1,2-bis(5-(2-butyloctyl)-4-chlorothiophen-2-yl)ethane-1,2-dione (**9**, 0.72 mmol) was used as the dione. The crude product was purified by column chromatography using MC/hexane (1/70, v/v) as eluent. Yield : 40% (yellow-orange oil). ¹H-NMR (400 MHz, CDCl₃) δ 8.12 (s, 1H), 7.84 (dd, J = 3.9, 1.1 Hz, 1H), 7.60 (dd, J = 5.0, 0.9 Hz, 1H), 7.55 (dd, J = 5.3, 1.1 Hz, 1H), 7.50 (q, J = 1.5 Hz, 1H), 7.34 (s, 1H), 7.28 (s, 1H), 7.22-7.18 (m, 2H), 2.81 (d, J = 7.3 Hz, 2H), 2.73 (d, J = 6.9 Hz, 2H), 1.78 (t, J = 5.3 Hz, 1H), 1.70 (t, J = 2.6 Hz, 1H), 1.35-1.27 (m, 32H), 0.90-0.86 (m, 12H). ¹³C-NMR (100 MHz, CDCl₃) δ 144.4, 143.2, 142.9, 142.5, 139.6, 137.5, 137.1, 137.0, 135.2, 135.0, 134.2, 132.4, 131.0, 129.9, 129.8, 129.5, 129.1, 128.1, 127.7, 127.0, 126.2, 123.1, 123.0, 39.4, 39.3, 33.5, 33.4, 33.1, 33.0, 32.7, 32.7, 32.0, 29.8, 29.7, 28.8, 28.8, 26.7, 23.1, 23.1, 22.8, 14.3, 14.2.

II-1.2.13. 2,3-bis(4-(2-butyloctyl)-5-chlorothiophen-2-yl)-6-chloro-5,8-di(thiophen-2-yl)quinoxaline (17)

The method to produce 2,3-bis(4-(2-butyloctyl)-5-chlorothiophen-2-yl)-6-chloro-

5,8-di(thiophen-2-yl)quinoxaline (**17**) was similar to the method used to produce **15**. Instead of 1,2-bis(5-(2-butyloctyl)thiophen-2-yl)ethane-1,2-dione (**8**), 1,2-bis(4-(2-butyloctyl)-5-chlorothiophen-2-yl)ethane-1,2-dione (**10**, 0.87 mmol) was used as the dione. The crude product was purified by column chromatography using MC/hexane (1/70, v/v) as eluent. Yield : 41% (yellow-orange oil). ¹H-NMR (400 MHz, CDCl₃) δ 8.10 (s, 1H), 7.81 (dd, J = 3.9, 1.1 Hz, 1H), 7.64 (dd, J = 5.3, 1.1 Hz, 1H), 7.58 (dd, J = 5.0, 0.9 Hz, 1H), 7.50 (q, J = 1.7 Hz, 1H), 7.31 (s, 1H), 7.26-7.24 (m, 2H), 7.19 (dd, J = 4.9, 3.8 Hz, 1H), 2.46 (dd, J = 19.2, 7.3 Hz, 4H), 1.57 (dd, J = 12.1, 5.3 Hz, 2H), 1.24 (s, 32H), 0.88-0.85 (m, 12H). ¹³C-NMR (100 MHz, CDCl₃) δ 144.3, 143.1, 139.5, 139.3, 139.3, 138.0, 137.5, 137.0, 135.1, 134.9, 134.2, 132.3, 131.2, 131.1, 130.9, 130.9, 130.4, 129.9, 129.4, 129.0, 128.2, 127.6, 127.0, 126.2, 38.6, 38.6, 33.3, 33.0, 32.7, 32.0, 29.8, 28.8, 26.5, 23.1, 22.8, 14.3, 14.2.

II-1.2.14. 5,8-bis(5-bromothiophen-2-yl)-2,3-bis(5-(2-butyloctyl)thiophen-2-yl)-6-chloroquinoxaline (18)

In a round bottom flask under N₂ protection, 2,3-bis(5-(2-butyloctyl)thiophen-2-yl)-6-chloro-5,8-di(thiophen-2-yl)quinoxaline (**15**, 1 equiv., 0.33 mmol) was dissolved in anhydrous THF at RT. After that, N-bromosuccinimide (2.1 equiv., 0.693 mmol) was added and stirred overnight at RT. And then, the mixture was extracted with dichloromethane. The organic layer was collected and dried over magnesium sulfate. The solvents were removed using rotary evaporator and the

crude product was purified by column chromatography using MC/hexane (1/50, v/v) as eluent. Yield : 70% (orange oil). ¹H-NMR (400 MHz, CDCl₃) δ 7.99 (t, J = 1.4 Hz, 1H), 7.52 (td, J = 2.6, 1.1 Hz, 1H), 7.40 (d, J = 3.7 Hz, 1H), 7.36 (dd, J = 5.0, 3.7 Hz, 2H), 7.14 (d, J = 4.1 Hz, 1H), 7.11 (d, J = 4.1 Hz, 1H), 6.70 (d, J = 4.1 Hz, 1H), 6.64 (d, J = 3.7 Hz, 1H), 2.80 (dd, J = 24.9, 6.6 Hz, 4H), 1.70 (d, J = 21.0 Hz, 2H), 1.30 (t, J = 14.6 Hz, 33H), 0.90-0.84 (m, 12H). ¹³C-NMR (100 MHz, CDCl₃) δ 150.8, 150.4, 146.1, 144.8, 139.2, 138.9, 138.5, 138.2, 135.9, 134.4, 133.7, 131.4, 130.3, 130.3, 129.4, 128.9, 128.3, 127.3, 126.7, 126.0, 118.0, 115.6, 40.1, 40.0, 34.9, 34.9, 33.4, 33.4, 33.1, 33.0, 32.0, 29.8, 29.0, 29.0, 26.8, 26.7, 23.1, 22.8, 14.3, 14.3. MALDI-TOF MS: m/z calcd, 987.52; found, 987.337 [M⁺].

II-1.2.15. 5,8-bis(5-bromothiophen-2-yl)-2,3-bis(5-(2-butylloctyl)-4-chlorothiophen-2-yl)-6-chloroquinoxaline (19)

The method to produce 5,8-bis(5-bromothiophen-2-yl)-2,3-bis(5-(2-butylloctyl)-4-chlorothiophen-2-yl)-6-chloroquinoxaline (**19**) was similar to the method used to produce **18**. 2,3-bis(5-(2-butylloctyl)-4-chlorothiophen-2-yl)-6-chloro-5,8-di(thiophen-2-yl)quinoxaline (**16**, 0.32 mmol) was used as the starting material. The crude product was purified by column chromatography using MC/hexane (1/50, v/v) as eluent. Yield : 61% (orange oil). ¹H-NMR (400 MHz, CDCl₃) δ 8.01 (q, J = 1.9

Hz, 1H), 7.49 (dd, J = 4.1, 0.9 Hz, 1H), 7.34-7.29 (m, 3H), 7.15-7.10 (m, 2H), 2.80 (dd, J = 24.7, 6.9 Hz, 4H), 1.81-1.76 (m, 2H), 1.37-1.24 (m, 32H), 0.91-0.84 (m, 12H). ¹³C-NMR (100 MHz, CDCl₃) δ 144.7, 143.5, 143.4, 143.1, 139.1, 137.8, 137.2, 136.5, 135.5, 134.6, 131.7, 131.5, 130.0, 129.9, 129.5, 129.0, 128.5, 128.0, 126.9, 123.2, 123.1, 118.3, 115.7, 39.5, 39.4, 33.5, 33.1, 33.1, 32.8, 32.0, 29.7, 28.9, 28.8, 26.7, 23.1, 22.8, 14.3. MALDI-TOF MS: m/z calcd, 1056.41; found, 1057.409 [M⁺].

II-1.2.16. 5,8-bis(5-bromothiophen-2-yl)-2,3-bis(4-(2-butylloctyl)-5-chlorothiophen-2-yl)-6-chloroquinoxaline (20)

The method to produce 5,8-bis(5-bromothiophen-2-yl)-2,3-bis(4-(2-butylloctyl)-5-chlorothiophen-2-yl)-6-chloroquinoxaline (**20**) was similar to the method used to produce **18**. 2,3-bis(4-(2-butylloctyl)-5-chlorothiophen-2-yl)-6-chloro-5,8-di(thiophen-2-yl)quinoxaline (**17**, 0.44 mmol) was used as the starting material. The crude product was purified by column chromatography using MC/hexane (1/50, v/v) as eluent. Yield : 68% (orange oil). ¹H-NMR (400 MHz, CDCl₃) δ 7.94 (s, 1H), 7.45 (d, J = 4.1 Hz, 1H), 7.31-7.26 (m, 3H), 7.16-7.08 (m, 2H), 2.47 (dd, J = 18.5, 7.1 Hz, 4H), 1.59 (q, J = 5.8 Hz, 2H), 1.26-1.23 (m, 32H), 0.86-0.83 (m, 12H). ¹³C-NMR (100 MHz, CDCl₃) δ 144.8, 143.4, 139.5, 139.4, 139.0, 137.8, 137.4, 136.7, 135.5, 134.5, 134.5, 131.7, 131.6, 131.5, 131.2, 130.7, 129.6, 129.1, 128.4, 127.9, 127.0,

118.2, 115.7, 38.7, 38.6, 33.3, 33.0, 33.0, 32.7, 32.0, 29.8, 28.8, 26.6, 23.2, 22.8, 14.3,
14.2. MALDI-TOF MS: m/z calcd, 1056.41; found, 1057.385 [M⁺].

II-1.3. General Procedure of Polymerization using Stille-Coupling Method with Palladium Catalyst

In a schlenk flask, BDT (0.20 mmol), dibrominated-quinoxaline monomer (0.20 mmol), tri(*o*-tolyl)phosphine (40% mol), and Pd₂(dba)₃ (5% mol) were dissolved in 10 mL dry chlorobenzene, DMF. The oxygen was removed by bubbling the solution with nitrogen for 15 minutes. The solution then was stirred at 110°C for 2 days under N₂ protection. 2-tribuylstannylthiophene and 2-bromothiophene were used as the end-capping agents aiming to stop the reaction. Both end-capping agents were added to the solution in sequence with 2 h' interval. After that, the polymer solution was precipitated in methanol and the solid was collected by filtration. The solid residue was further purified by Soxhlet extraction with methanol, acetone, hexane, and chloroform. The polymer in chloroform fraction was recovered by precipitation into methanol again, Finally, the polymer was dried in a vacuum oven at 55 °C.

II-1.3.1. PB-Q

In a Schlenk flask, compound **18** (0.14 mmol, 1 equiv.), (4,8-bis(4-chloro-5-(2-ethylhexyl)thiophen-2-yl)benzo[1,2-b:4,5-b']dithiophene-2,6-

diyl)bis(trimethylstannane) (0.14 mmol, 1 equiv.), tri(*o*-tolyl)phosphine (0.056 mmol, 40 mol%) and tris(dibenzylideneacetone)dipalladium (Pd₂(dba)₃, 0.007 mmol, 5 mol%) were mixed together in anhydrous mixed solvent of chlorobenzene (4 mL) and DMF (1 mL). After N₂ bubbling for 15 min, the solution was stirred at 110 °C for 48 h under N₂ protection. The polymerization was finished by adding two end-capping agents of 2-tributylstannylthiophene and 2-bromothiophene at 2h interval. The polymer solution was precipitated in methanol and the solid was collected by filtration. The solid residue was further purified by Soxhlet extraction with methanol, acetone, hexane, and chloroform. The polymer in chloroform fraction was recovered by precipitation into methanol again. Finally, the polymer was dried in a vacuum oven at 55 °C. Yield = 95% (dark red solid). ¹H-NMR (400 MHz, CDCl₃) δ 7.26-8.79 (9H), 6.50-7.22 (4H), 2.43-3.25 (8H), 1.62-1.92 (4H), 1.10-1.52 (48H), 0.74-1.03 (24H). Molecular weight by GPC: number-average molecular weight (M_n) = 64.37 KDa, polydispersity index (PDI) = 2.63.

II-1.3.2. PB-Q-4Cl

The same procedure used to prepare **PB-Q** was used to produce **PB-Q-4Cl**. Instead of compound **18**, compound **19** was used as the alternative dibrominated quinoxaline monomer. Yield = 92% (dark red solid). ¹H-NMR (400 MHz, CDCl₃) δ 7.27-8.13 (9H), 6.91-7.19 (2H), 2.30-3.61 (8H), 1.64-1.90 (4H), 1.14-1.40 (48H), 0.73-0.94 (24H). Molecular weight by GPC: number-average molecular weight (M_n)

= 37.48 KDa, polydispersity index (PDI) = 3.15.

II-1.3.3. PB-Q-5Cl

The same procedure used to prepare **PB-Q** was used to produce **PB-Q-5Cl**. Instead of compound **18**, compound **20** was used as the alternative dibrominated quinoxaline monomer. Yield = 89% (dark red solid). ¹H-NMR (400 MHz, CDCl₃) δ 7.26-7.90 (9H), 6.74-7.19 (2H), 2.26-3.25 (8H), 1.68-1.91 (4H), 1.19-1.39 (49H), 0.82-0.95 (24H). Molecular weight by GPC: number-average molecular weight (Mn) = 32.25 KDa, polydispersity index (PDI) = 3.52.

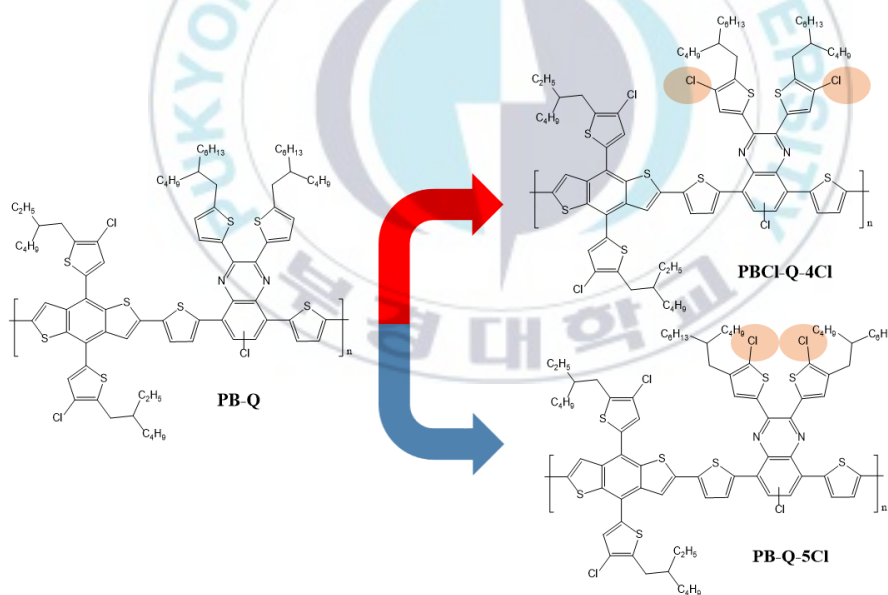
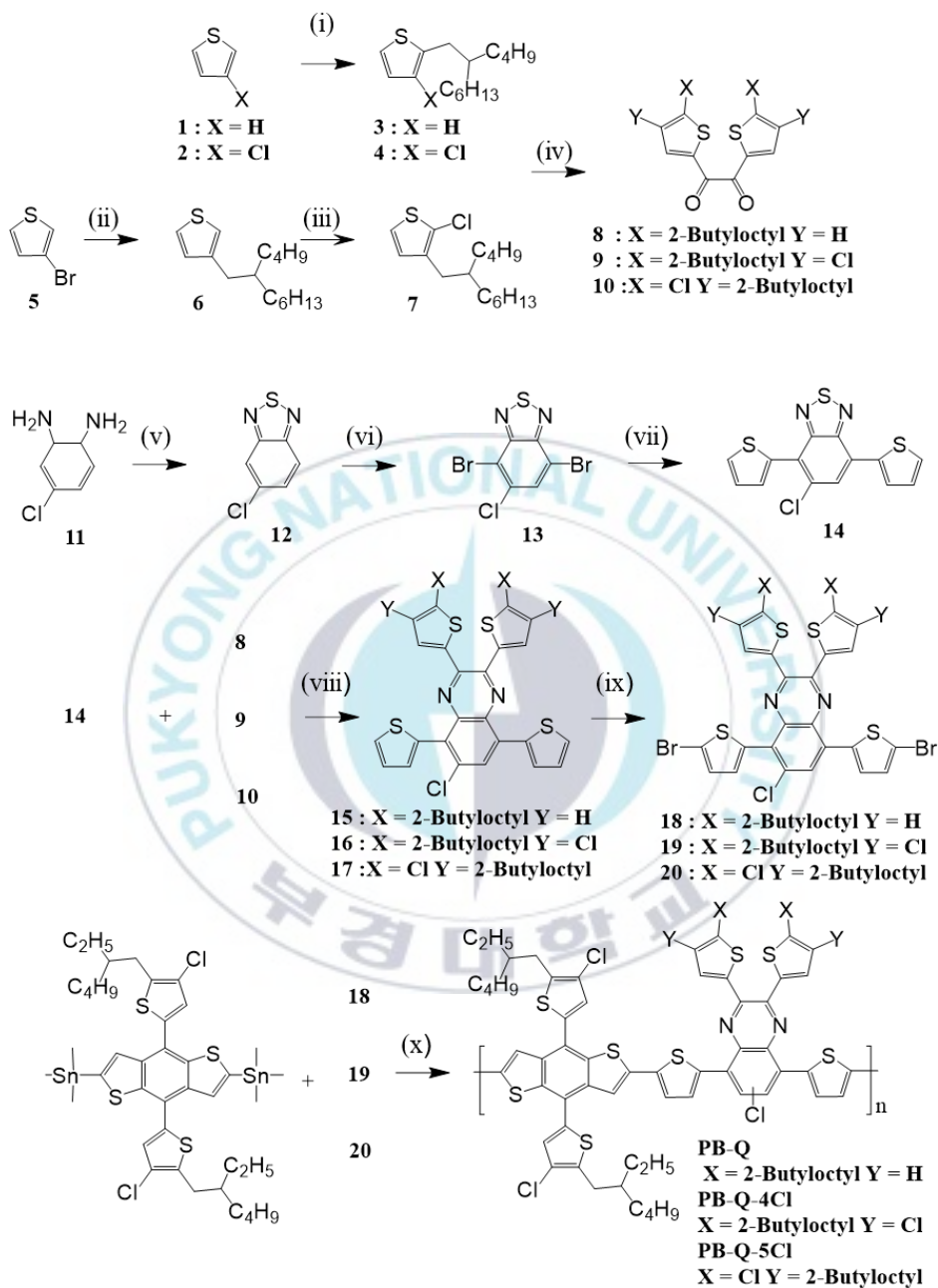


Figure II-1. Chemical structure of **PB-Q-Cl** Series.



Scheme 1. Synthetic routes of PB-Q-Cl Series.

II-1.4. Fabrication and Analysis of Photovoltaic Devices

The polymer was fabricated on the conventional-type of polymer solar cells device. The device structure consisted of ITO/PEDOT:PSS/PB-Q-Cl Series:Y6 /PDINO/Al. The ITO glass substrate was cleaned via sequential sonication with deionized water, acetone, and 2-propanol each for 10 minutes. After drying the substrates were subjected to UV-oxone treatment for 15 min. Subsequently, the SnO₂ diluted solution was spin-coated at 3000 rpm for 30 s and then thermal annealed at 150 °C for 15 minutes. Prior to the active film coatings the substrates were subjected to the UV treatment for 10 minutes. A solution of the polymers with Y6 was made by dissolving in CHCl₃ with 0.5% DIO. The blended solution was spin-coated at 2000-3000 rpm for 30 s to achieve an active layer thickness of 100 nm. Post process of spin-coating, the substrates were taken under a pressure of <10⁻⁶ Torr, with 8 nm and 100 nm thickness of MoO_x and Ag metal electrode, respectively using thermal evaporator.

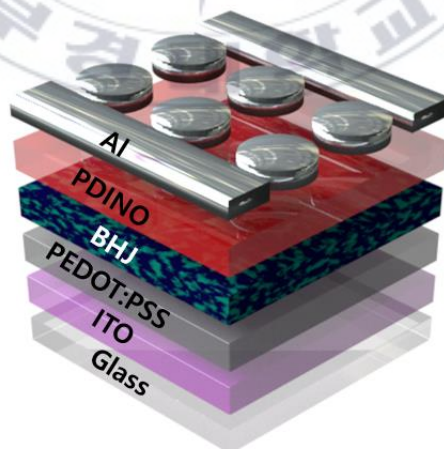


Figure II-2. Device structure of PSCs

II-2. Result and Discussion

II-2.1. Synthesis and Physical Properties of Polymers

The preparation routes for the monomers and polymers are shown in Scheme 1, and their synthetic routes and analytical results are described in the previous experimental section. First, the reaction of starting materials afforded thiophene derivatives was performed. Second, α -diketone was prepared via the Friedel–Crafts reaction of first step intermediates in the presence of oxalyl chloride. Third, the zinc-mediated reduction and condensation were performed on 4,7-dibromo[*c*][1,2,5]thiadiazole derivatives to synthesize dibrominated quinoxaline monomers with strong electron-withdrawing Cl substituents. Finally, the polymerization of a chlorinated BDT donor with dibrominated quinoxaline under the Stille coupling condition yielded the target D–A-type quinoxaline-based polymers, i.e., **PB-Q**, **PB-Q-4Cl** and **PB-Q-5Cl**, respectively. In this synthetic strategy, a unique polymeric architecture, in which the electron-donating BDT and different position chlorine substituents are located in the horizontal and vertical directions of the electron-accepting quinoxaline unit, respectively, was achieved. The formation of the D-A structure not only strengthened the structural uniqueness of the target polymers, but also induced broad light absorption and reduced the bandgap through the facile electron transfer process in both directions. The molecular weights of the polymers were analyzed via gel permeation chromatography using tetrahydrofuran (THF) as the eluent. The number-average molecular weight and polydispersity index

of **PB-Q**, **PB-Q-4Cl** and **PB-Q-5Cl** were 64.37 kDa and 2.63, 37.48 kDa and 3.15, and 32.25 kDa and 3.52, respectively. These polymers exhibited good solubility in various organic solvents such as chloroform, toluene, and chlorobenzene, owing to the existence of 2-ethylhexyl and 2-butyloctyl side chains on BDT and quinoxaline units, respectively.

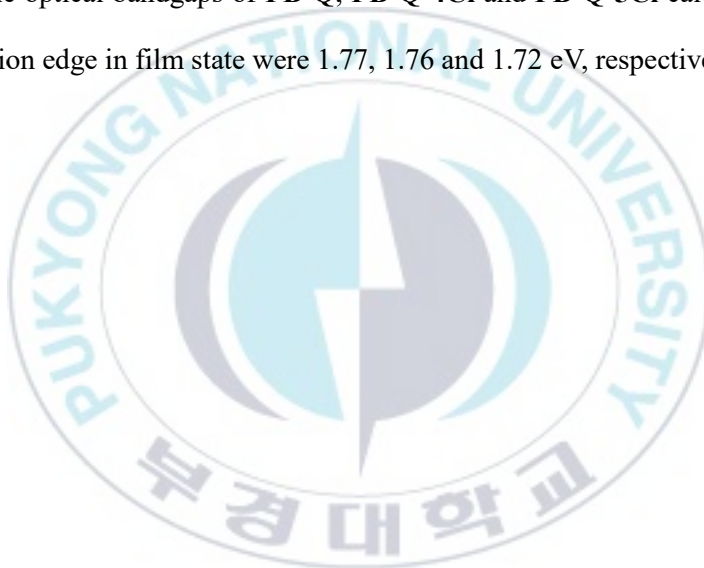
Table II-1. Molecular weight of the polymers

Polymer	M_n (kDa)	M_w (kDa)	PDI
PB-Q	64.37	169.29	2.63
PB-Q-4Cl	37.48	118.06	3.15
PB-Q-5Cl	32.25	113.52	3.52

II-2.2. Optical and Electrochemical Properties of Polymers

The optical properties of the polymers were analyzed using ultraviolet–visible (UV–Vis) spectroscopy. As shown in **Figures II-2**, all polymers exhibited three broad absorption peaks in both the chloroform solution and film on the glass substrate. The peak in the shorter wavelength region of 300–470 nm was associated with the π – π^* transitions of the conjugated backbones, whereas that at longer wavelength regions of 470–700 nm originated from the formation of an ICT state between the donor and acceptor units in the polymer chains. The molar extinction coefficients (ϵ) in the ICT region of **PB-Q**, **PB-Q-4Cl** and **PB-Q-5Cl** in chloroform solution were 5.80×10^4 , $5.40 \times 10^4 \text{ M}^{-1} \text{ cm}^{-1}$ and $5.30 \times 10^4 \text{ M}^{-1} \text{ cm}^{-1}$, respectively.

The maximum absorption peak of **PB-Q-5Cl** was red shifted by approximately 8 nm compared with that of other polymers. Interestingly, the ε value of **PB-Q** at longer wavelengths compared with that of other polymers shows highest value caused by the drawbacks of more electron-withdrawing Cl units. The three polymers exhibited good complementary light absorption spectra with an *n*-type Y6 acceptor in the film state, which is beneficial for improving the photovoltaic properties of the devices. In addition, the optical bandgaps of **PB-Q**, **PB-Q-4Cl** and **PB-Q-5Cl** calculated from the absorption edge in film state were 1.77, 1.76 and 1.72 eV, respectively



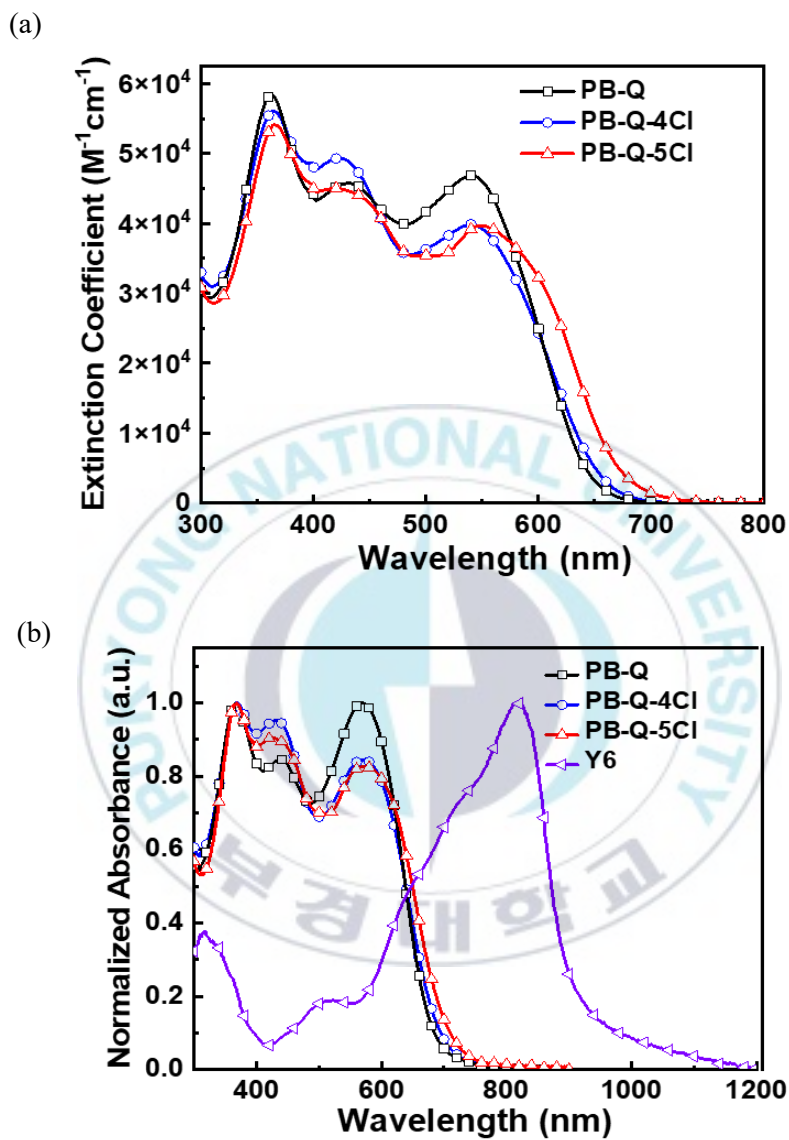


Figure II-3. UV-Visible spectra of polymer in (a) chloroform solution and (b) film-state on glass substrate (spectra are offset for clarity)

The electrochemical properties of the polymers were analyzed using cyclic voltammetry (CV) measurements with a ferrocene (Fc)/ferrocenium (Fc⁺) external standard. The HOMO and LUMO energy levels were determined from the onset oxidation and reduction potentials, respectively, in the cyclic voltammograms. The calculated HOMO/LUMO energy levels of **PB-Q**, **PB-Q-4Cl** and **PB-Q-5Cl** were -5.47/-3.16, -5.58/-3.25 and -5.54/-3.40 eV, respectively. The different position of Cl unit can induce a significant reduction in both the HOMO and LUMO energy levels of **PB-Q-4Cl** and **PB-Q-5Cl** compared with those of **PB-Q**. In addition, the electrochemical bandgaps of **PB-Q**, **PB-Q-4Cl** and **PB-Q-5Cl** estimated from the difference between their HOMO and LUMO energy levels were 2.33, 2.33 and 2.14 eV, respectively. The electrochemical bandgap of the polymers exhibited the same trend as the optical bandgaps. The optical and electrochemical properties of the polymers are listed in **Table II-2**. Based on the results, it was discovered that the different position of Cl moiety in the quinoxaline acceptor unit slightly affected the optical and electrochemical properties of the corresponding D–A-type polymers.

Table II-2. Optical and electrochemical properties of the **PB-Q-Cl** Series

Polymers	ε ($M^{-1} cm^{-1}$)	E_{gap}^{opt} (eV) ^a	$\lambda_{max}^{solution}$ (nm) ^b	HOMO (eV) ^c	LUMO (eV) ^d	E_{gap}^{elec} (eV) ^e
PB-Q	5.80×10^4	1.77	362, 540	-5.47	-3.16	2.33
PB-Q4Cl	5.40×10^4	1.76	366, 541	-5.58	-3.25	2.33
PB-Q5Cl	5.30×10^4	1.71	367, 554	-5.54	-3.40	2.14

^aEstimated from the absorption edge in the film state. ^bMaximum absorption wavelengths of polymers in chloroform solution. ^cEstimated from the oxidation onset potential. ^dEstimated from the reduction onset potential. ^eCalculated from the oxidation and reduction onset potentials in the CV curves.

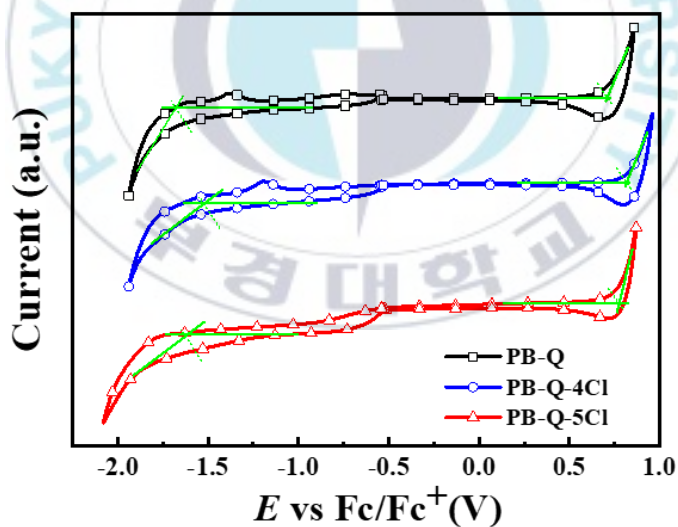


Figure II-4. Cyclic voltammograms of **PB-Q-Cl** polymers

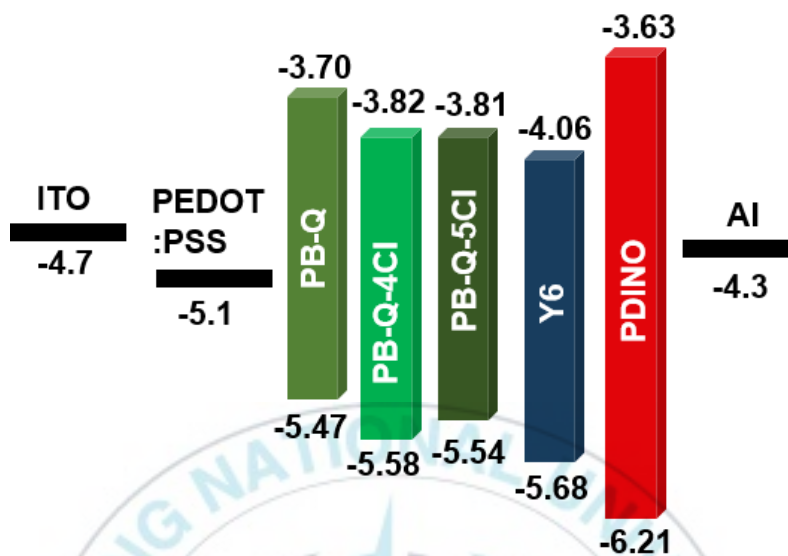


Figure II-5. Energy level diagram of all materials in the Conventional-type devices: HOMO was obtained from CV results and LUMO was obtained from optical band gap.

II-2.3. Theoretical calculation

Density functional simulations using the Gaussian 09 program at the B3LYP/6-31G** level were performed to estimate the optimized geometries and frontier molecular orbitals of the polymers[25]. To reduce complicated computational calculations, 2-ethylhexyl chains on BDT donors and long alkyl chains on polymer backbones were simplified to the shortest methyl group and small dimer unit, respectively. In the optimized geometries, the dihedral angles between the thiophene unit and quinoxaline acceptor in the polymer backbone changed significantly from

54.6° in chlorine atom adjacent position and 23.5° in chlorine atom far position site. From the viewpoint of frontier molecular orbitals, similar characteristic features were observed in the three polymers. The HOMO wave functions of all the polymers were localized on the BDT units, whereas their LUMO wave functions were delocalized along the quinoxaline units. However, the HOMO and LUMO energy levels of the polymers were changed significantly by the position of electron-withdrawing substituent on the quinoxaline acceptor. The simulated HOMO/LUMO energy levels of **PB-Q**, **PB-Q-4Cl** and **PB-Q-5Cl** were -5.01/-2.65 eV, -5.14/-2.76 eV and -5.13/-2.77 eV, respectively. Therefore, both the HOMO and LUMO energy levels of **PB-Q**, **PB-Q-4Cl** and **PB-Q-5Cl** were exhibited relatively different values for introducing Cl moiety and each position. As experimentally observed based on the HOMO/LUMO energy levels of the polymers using CV measurements, the theoretical HOMO/LUMO energy levels of the polymers reduced owing to the substitution of Cl atom and different position.

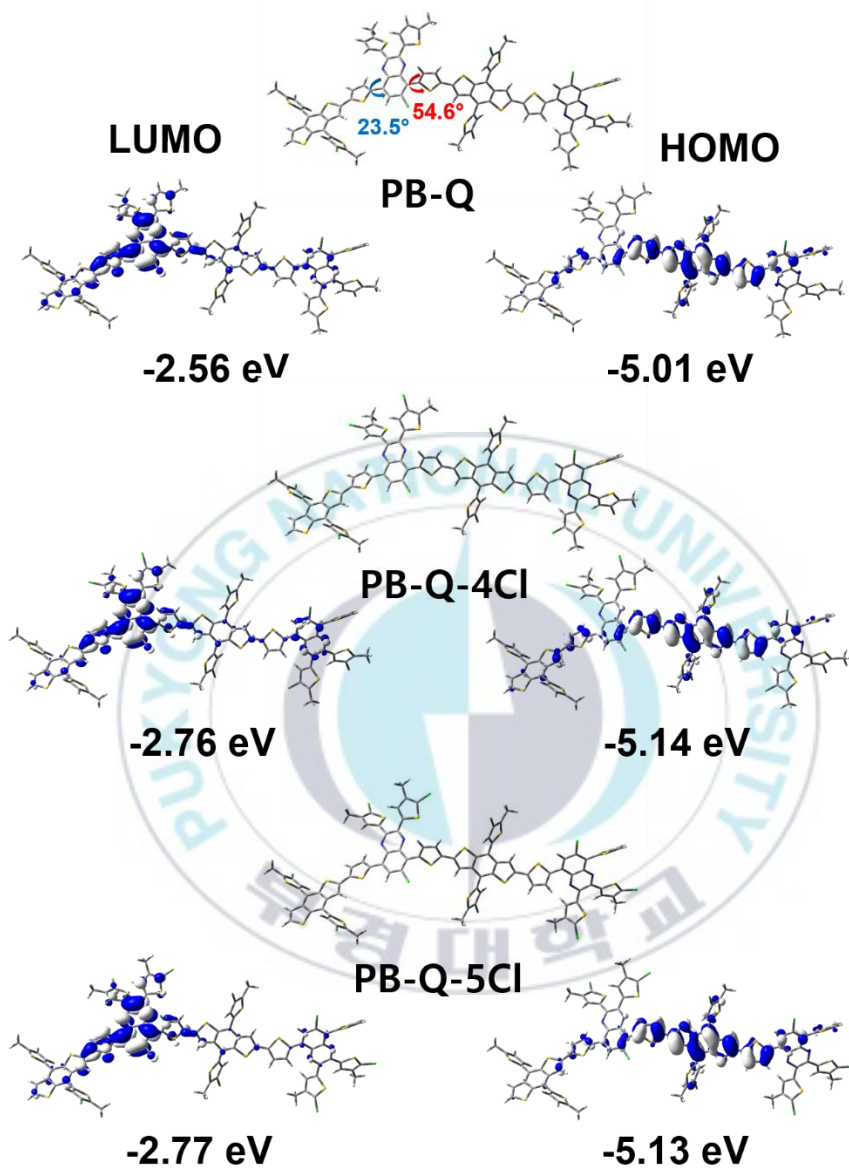


Figure II-6. Frontier molecular orbitals of two-repeating unit models with energy levels calculated at the B3LYP/6-31G** level for **PB-Q-Cl** Polymers

II-2.4. Photovoltaic Characteristics

The photovoltaic characteristics of the PB-Q-Cl series were investigated by fabricating conventional-type PSCs with the ITO/PEDOT: PSS/Active layer:Y6/PDINO/Al structure. After measuring the devices under various fabrication parameters, the optimum fabrication conditions were determined. Especially, the devices based on PB-Q-Cl series polymers, and the polymer:Y6 blend ratios of 1:1 as the same condition. During the casting of the active layer, 1.0 vol% of 1,8-diiodooctane was used as a processing additive. The current density-voltage ($J-V$) curves of the PSCs under optimum conditions and the irradiation of 1.0 sun are shown in **Figure II-6a**, and the photovoltaic parameters are listed in **Table II-3**. The PCE of the device based on **PB-Q** was limited to 12.44%, while that of the devices based on the C-4 position chlorinated polymer, **PB-Q-4Cl**, increased to 12.95%. The introduction of C-4 position chlorine atom not only extended absorption region but also reduced the HOMO energy level of the polymer. This enhanced the short-circuit current density (J_{SC}) and V_{OC} of the device, thus increasing its PCE. Interestingly, although the PCE value of the device based on **PB-Q-Cl** was lower than that of the device based on **PB-Q**, it was significantly lower than that of the device based on **PB-Q-4Cl**. Because of the HOMO energy levels of **PB-Q-5Cl**, the corresponding device showed the highest V_{OC} value of 0.82 V. However, the J_{SC} and fill factor (FF) of the device based on **PB-Q-5Cl** were lower than those of the device based on **PB-Q**. Therefore, it can be stated that the position of chlorine units in quinoxaline-based

polymers dramatically affects their photovoltaic characteristics. **Figure II-6b** shows the external quantum efficiency (EQE) curves of all the devices under optimum conditions. As can be observed from the **Figure II-6b**, the devices exhibited good photon responses over the absorption range of 300–950 nm.

Table II-3. Best photovoltaic parameters of the PSCs. Values in parentheses represent average value of photovoltaic parameters for each device

Polymer	J_{sc} (mA cm ⁻²)	J_{EQE} (mA cm ⁻²)	V_{oc} (V)	FF (%)	PCE (%)
PB-Q	26.32	26.10	0.76	62.16	12.44
PB-Q4Cl	24.90	24.04	0.82	63.63	12.95
PB-Q5Cl	24.47	23.66	0.79	61.29	11.82

^aThe series resistance estimated from the corresponding best device.

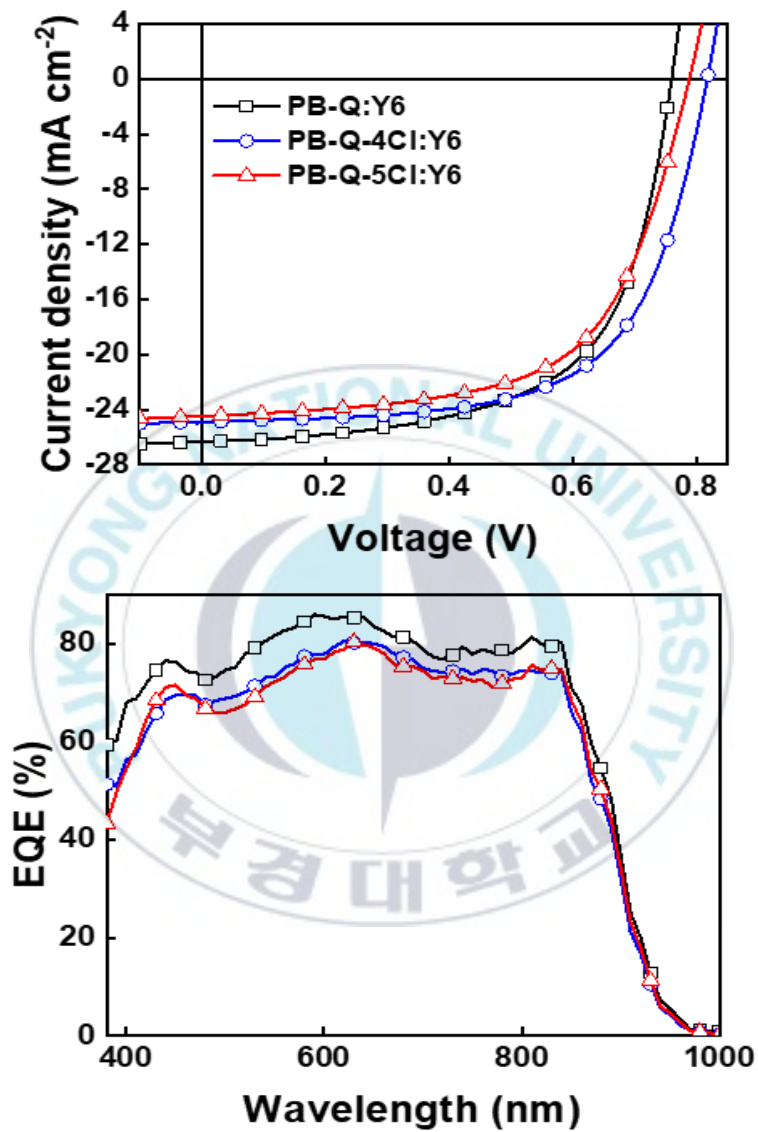


Figure II-7. (a) J-V curve of PSCs under 1.0 sun condition and (b) EQE spectra of PSCs based on PB-Q-Cl Series.

Table II-4. SCLC characterization of the PSCs.

Polymer	G_{\max} ($10^{28} \text{ m}^{-3} \text{ s}^{-1}$)	P (E,T) _{SC} (%)	μ_h (10^{-4} cm^2 $\text{V}^{-1} \text{ s}^{-1}$)	μ_e (10^{-4} cm^2 $\text{V}^{-1} \text{ s}^{-1}$)	μ_h/μ_e
PB-Q	1.67	98.23	5.80	2.80	2.07
PB-Q4Cl	1.58	98.96	6.00	3.60	1.67
PB-Q5Cl	1.66	92.94	7.00	2.40	2.92

To further evaluate the charge carrier transfer properties of the active blends in single-carrier devices, J - V characteristics of the electron- and hole-only devices were analyzed with a well-known space-charge-limited-current (SCLC) model. The structures of the devices employed were ITO/PEDOT:PSS/active layer/Au and ITO/PDINO/active layer/LiF/Al for the hole- and electron-only devices, respectively. The characteristic J - V curves of the single-carrier devices are shown in **Figure II-7** and **Table II-4**. The electron (μ_e) and hole (μ_h) mobilities of the **PB-Q:Y6** device and **PB-Q4Cl:Y6** device were measured to be 2.8×10^{-4} / 5.8×10^{-4} and 3.6×10^{-4} / $6.0 \times 10^{-4} \text{ cm}^2 \text{ V}^{-1} \text{ s}^{-1}$, whereas those of the **PB-Q5Cl:Y6** device were 2.4×10^{-4} / $7.0 \times 10^{-4} \text{ cm}^2 \text{ V}^{-1} \text{ s}^{-1}$, respectively. The introduction of Cl atom in polymer donors with the different position can induce the detrimental effects on the charge-carrier mobilities of the devices such as the increase in undesirable charge recombination process. The decreased charge transfer ability of the **PB-Q5Cl:Y6** device might have contributed to the lower J_{SC} values. Owing to the high μ_e and μ_h values of **PB-Q-4Cl:Y6**, high values of J_{SC} and FF were observed.

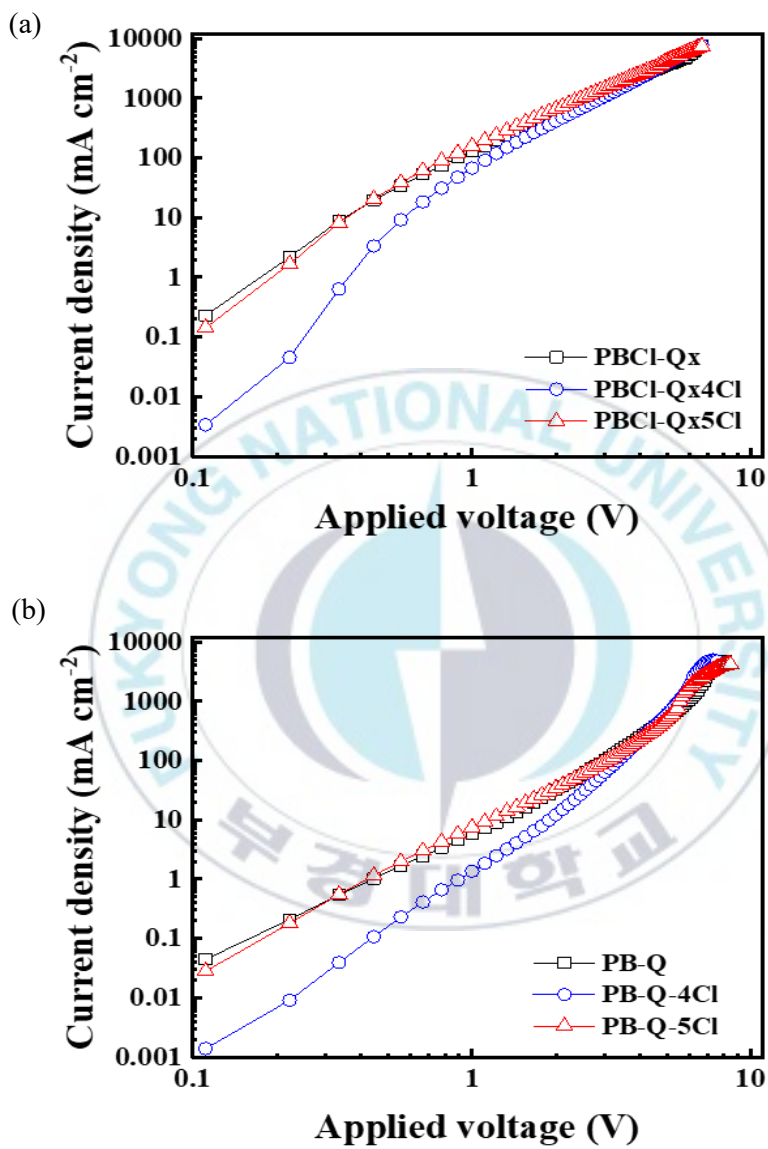


Figure II-8. J-V curves of (a) the electron-only and (b) hole-only devices

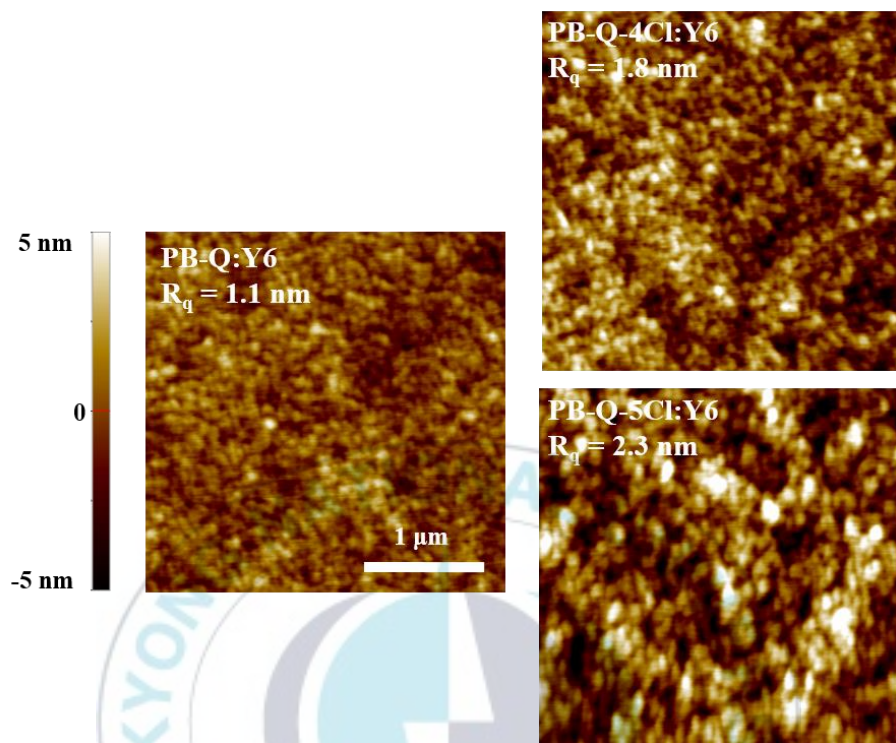


Figure II-9. AFM images of **PB-QCl** Seires polymer blend film with Y6.

To investigate the surface morphology of the active layer, atomic force microscopy (AFM) measurements were measured in the tapping mode, and the resultant images are shown in **Figure II-8**. The PB-Q-Cl polymers:Y6 blend films based on different polymers showed distinct morphological differences. A homogeneous spherical morphology and clear domain boundary was observed for the blend film comprising **PB-Q-4Cl**, whereas the film comprising **PB-Q** exhibited the obscuring domain size morphology. Consequently, the blend film comprising **PB-Q-4Cl** exhibited a relatively clear film and contained bicontinuous interpenetrating networks, as compared with the film comprising **PB-Q**. The

obscuring domain size of the film comprising **PB-Q** yielded a low root-mean-square (RMS) surface roughness of 1.1 nm, compared with that of the film comprising **PB-Q-4Cl** (RMS value of 3.8 nm). In addition, the introduction of C-5 position chlorine atoms in the polymer chain resulted in the formation of larger D/A domains, which hindered efficient exciton dissociation and charge transport. So, **PB-Q-5Cl** film yielded a highest RMS value of 2.3 nm.



Chapter III. Conclusion.

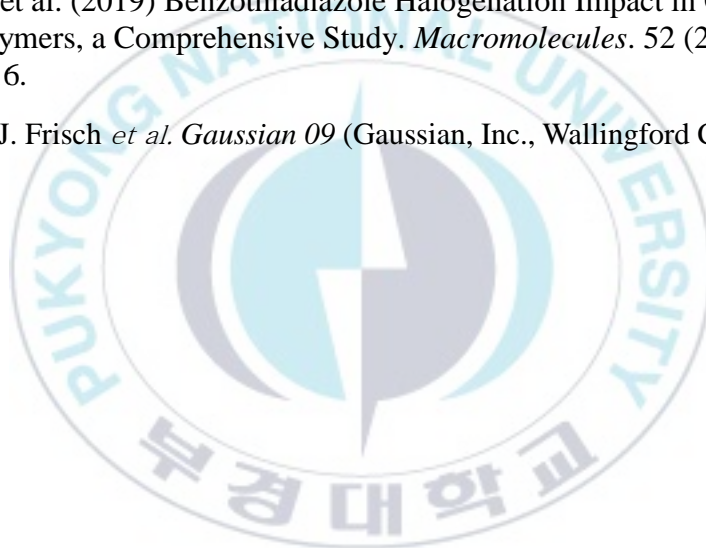
Three quinoxaline-based D–A type conjugated polymers of **PB-Q**, **PB-Q-4Cl** and **PB-Q-5Cl**, in which the different position of Cl unit was selectively introduced, respectively, were synthesized via the Stille coupling reaction to investigate their effects on the photovoltaic performances of the polymers. Owing to the electron-withdrawing drawbacks of the Cl units, **PB-Q-4Cl** and **PB-Q-5Cl** exhibited a lower ε value in the ICT region. Conversely, the advantage of the Cl units, a lower HOMO energy level compared with **PB-Q**. Under these conditions, the accompanying enhancement in the J_{sc} , V_{oc} , and PCE of the **PB-Q-4Cl**-based device can be expected. Therefore, the highest PCE of 12.95% was achieved from the **PB-Q-4Cl**-based device, which exhibited a J_{sc} of 24.90 mA/cm², V_{oc} of 0.82 V, and FF of 0.63. The PCE of the **PB-Q**-based device was limited to 12.44%, with a J_{sc} of 26.32 mA/cm², V_{oc} of 0.76 V, and FF of 0.62. In case of **PB-Q-5Cl**, it was clear that the J_{sc} , FF, and PCE of the **PB-Q-5Cl**-based device were inferior to those of the **PB-Q**-based device. The significant reduction in the J_{sc} and FF of the **PB-Q-5Cl**-based device was attributable to the unfavorable large domain-induced charge recombination and charge carrier transport kinetics. Therefore, the different position incorporating of electron-withdrawing substituents on the quinoxaline-based polymers must be controlled well because their photovoltaic properties are affected dramatically. This study provides valuable information regarding the position effect of withdrawing groups on the D–A-type quinoxaline-based polymers.

References

- [1] Dimitrakopoulos, C.D. and Mascaro, D.J. (2001) by C. D. Dimitrakopoulos D. J. Mascaro. 45 (1), 11–27.
- [2] Kunkel, C., Margraf, J.T., Chen, K., Oberhofer, H., and Reuter, K. (2021) Active discovery of organic semiconductors. *Nature Communications*. 12 (1), 1–11.
- [3] Lu, G. (2006) 2006.12.08. Organic Semiconductor. (585), 2–5.
- [4] Bronstein, H., Nielsen, C.B., Schroeder, B.C., and McCulloch, I. (2020) The role of chemical design in the performance of organic semiconductors. *Nature Reviews Chemistry*. 4 (2), 66–77.
- [5] Huang, Y., Elder, D.L., Kwiram, A.L., Jenekhe, S.A., Jen, A.K.Y., Dalton, L.R., et al. (2021) Organic Semiconductors at the University of Washington: Advancements in Materials Design and Synthesis and toward Industrial Scale Production. *Advanced Materials*. 33 (22), 1–23.
- [6] Singh, T.B. and Sariciftci, N.S. (2006) Progress in plastic electronics devices. *Annual Review of Materials Research*. 36 (5), 199–230.
- [7] Giovanella, U., Pasini, M., and Botta, C. (2016) Organic Light-Emitting Diodes (OLEDs): Working Principles and Device Technology. .
- [8] Bernède, J.C. (2008) Organic photovoltaic cells: History, principle and techniques. *Journal of the Chilean Chemical Society*. 53 (3), 1549–1564.
- [9] Marinova, N., Valero, S., and Delgado, J.L. (2017) Organic and perovskite solar cells: Working principles, materials and interfaces. *Journal of Colloid and Interface Science*. 488 373–389.
- [10] Arbouch, I., Karzazi, Y., and Hammouti, B. (2014) Organic photovoltaic cells: Operating principles, recent developments and current challenges – review. *Physical and Chemical News*. 72 (4), 73–84.
- [11] Wardani, R.P., Jeong, M., Lee, S.W., Whang, D.R., Kim, J.H., and

- Chang, D.W. (2021) Simple methoxy-substituted quinoxaline-based D-A type polymers for nonfullerene polymer solar cells. *Dyes and Pigments*. 192 (April), 109346.
- [12] Lee, S.W., Jeong, M., Whang, D.R., Kim, J.H., and Chang, D.W. (2020) Effect of Fluorine Atom on Photovoltaic Properties of Triphenylamine-Substituted Quinoxaline-Based D-A Type Polymers. *Macromolecular Research*. 28 1297–1303.
- [13] Sagita, C.P., Lee, J.H., Lee, S.W., Whang, D.R., Kim, J.H., and Chang, D.W. (2021) Enhanced photovoltaic performance of quinoxaline-based donor-acceptor type polymers with monocyano substituent. *Journal of Power Sources*. 491 (October 2020), 229588.
- [14] Najam, S. and Kumar, B. (2018) Organic Solar Cell: Operating Principle, Performance Parameters, Structures and Its Advantages. *2018 5th IEEE Uttar Pradesh Section International Conference on Electrical, Electronics and Computer Engineering, UPCON 2018*.
- [15] . V.K.A. (2014) Organic Solar Cells: Principles, Mechanism and Recent Dvelopments. *International Journal of Research in Engineering and Technology*. 03 (09), 338–341.
- [16] Liu, S., Yuan, J., Deng, W., Luo, M., Xie, Y., Liang, Q., et al. (2020) High-efficiency organic solar cells with low non-radiative recombination loss and low energetic disorder. *Nature Photonics*. 14 (5), 300–305.
- [17] Liu, Q., Jiang, Y., Jin, K., Qin, J., Xu, J., Li, W., et al. (2020) 18% Efficiency organic solar cells. *Science Bulletin*. 65 (4), 272–275.
- [18] Zhu, C., Meng, L., Zhang, J., Qin, S., Lai, W., Qiu, B., et al. (2021) A Quinoxaline-Based D–A Copolymer Donor Achieving 17.62% Efficiency of Organic Solar Cells. *Advanced Materials*. 33 (23), 1–9.
- [19] Zhang, T., An, C., Cui, Y., Zhang, J., Bi, P., Yang, C., et al. (2021) A Universal Nonhalogenated Polymer Donor for High-Performance Organic Photovoltaic Cells. *Advanced Materials*. 2105803 1–8.
- [20] Zhao, Q., Lai, H., Chen, H., Li, H., and He, F. (2021) H- And J-aggregation inspiring efficient solar conversion. *Journal of Materials Chemistry A*. 9 (2), 1119–1126.

- [21] Qi, B. and Wang, J. (2013) Fill factor in organic solar cells. *Physical Chemistry Chemical Physics*. 15 (23), 8972–8982.
- [22] Padilla, M., Michl, B., Thaidigsmann, B., Warta, W., and Schubert, M.C. (2014) Short-circuit current density mapping for solar cells. *Solar Energy Materials and Solar Cells*. 120 (PART A), 282–288.
- [23] Yang, M.H., Ko, S.J., An, N.G., Whang, D.R., Lee, S.H., Ahn, H., et al. (2020) Roll-to-roll compatible quinoxaline-based polymers toward high performance polymer solar cells. *Journal of Materials Chemistry A*. 8 (47), 25208–25216.
- [24] Olla, T., Ibraikulov, O.A., Ferry, S., Boyron, O., Méry, S., Heinrich, B., et al. (2019) Benzothiadiazole Halogenation Impact in Conjugated Polymers, a Comprehensive Study. *Macromolecules*. 52 (21), 8006–8016.
- [25] M. J. Frisch *et al.* *Gaussian 09* (Gaussian, Inc., Wallingford CT, 2009).



Acknowledgements

먼저, 대학원 과정 2년동안 많은 가르침을 주시고 제가 공부할 수 있도록 최선을 다해 가르침을 주신 장재원 교수님께 진심으로 감사드립니다. 또, 함께 연구를 진행하며 많은 도움과 가르침을 주신 이보람 교수님께도 감사합니다. 교수님들께서 주신 가르침 덕분에 연구뿐만 아니라 많은 부분에서 영감을 얻고 긍정적인 영향으로 많이 배울 수 있었다고 생각합니다. 그리고 대학 생활 동안 많은 가르침을 주신 문명준 교수님, 이근대 교수님, 박진환 교수님, 진영읍 교수님, 손민영 교수님, 조계용 교수님 그리고 채수종 교수님 정말 감사합니다.

2년의 석사과정 동안 믿고 지지해주신 부모님 그리고 친구들에게도 고마움을 표합니다. 덕분에 많은 배움을 얻고 한층 더 성장할 수 있었다고 생각합니다. 대학원을 시작하고 가장 먼저 후배로 들어와주었던 지민이에게 힘든 시기에 많은 도움을 주고 고민을 들어줘서 많은 도움이 되었어서 고마워요. 그리고 석사과정을 시작할 수 있고 연구에 많은 도움을 주었던 준태형님에게 감사의 말씀을 드립니다. 덕분에 새로운 공부를 다양하게 할 수 있었고 재미있는 석사과정을 진행할 수 있었습니다. 또, 같이 연구를 진행하였던 많은 연구자분들 및 교수님들께도 감사의 인사를 드립니다. 마지막으로, 석사과정 중 여러 도움을 주신 학과 사무실 안현정, 임혜원 선생님 항상 많은 도움을 주셔서 원활히 석사생활을 할 수 있었던 것 같습니다 감사합니다. 또, 지금도 열심히 연구를 진행하고 있는 실험실 후배 유경, dinda, 준수, 수연이에게 항상 바쁘다는 핑계로 많은 도움을 주지 못했던 것 같아 미안하고 학업을 잘 마무리 했으면 좋겠다. 석사과정동안 저에게 많은 가르침을 주시고 도와주신 모든 분들께 다시 한번 감사의 말씀을 드립니다. 정말 감사합니다.